ANALYZING THE MORPHOLOGY OF HEMOZOIN IN DRUG RESISTANT *PLASMODIUM* & QUANTIFYING THE COMPARTMENTAL KINETICS OF HEMOZOIN DURING CLEARANCE OF INFECTION

By

Abeer A. Sayeed

A thesis submitted to the Johns Hopkins University in conformity with the requirements for the degree of Master of Science

Baltimore, Maryland

April, 2019

ABSTRACT

Malaria infection by *Plasmodium* parasites poses a significant public health burden globally. During the parasite's erythrocytic life cycle stages, it produces hemozoin, an inert, crystalline by-product of hemoglobin degradation, to avoid oxidative stress. This process is essential for parasite survival and is therefore a target for antimalarials. In this thesis, we explore the effect of single nucleotide polymorphisms (SNPs) in drug resistant parasites on hemozoin morphology. We found that parasites with compressed trophozoite stages in a ring-stage artemisinin resistant strain (C580Y) harboring a Kelch-13 propeller mutation, produce significantly smaller sized hemozoin crystals than the isogenic susceptible strain (CamWT). Smaller sized hemozoin crystals were also observed in a chloroquine resistant strain (FCB) as compared to its isogenic chloroquine sensitive strain (106/1). We did not observe a significant difference in non-isogenic drug sensitive and resistant strains, suggesting that a SNP conferring resistance may be sufficient to alter hemozoin morphology. From these data we predict that parasites may alter their hemozoin nucleation processes as a stress response in order to overcome drug pressure.

Current malarial diagnostics have their limitations and therefore need improvement. Hemozoin is being explored as a potential biomarker to be used in malaria diagnostics. Therefore, it is essential to understand the kinetics of hemozoin during infection and clearance in order to develop appropriate tools to detect malaria infection using hemozoin. Additionally, in this thesis, we developed a sensitive luminescence assay to quantify hemozoin, with the ultimate goal of being able to detect and quantify hemozoin within the RBC and plasma compartments of whole blood. In *P. berghei*

infected white mice, we quantified hemozoin in the livers, spleens, whole blood, RBC, and plasma fractions to observe the kinetics of hemozoin during clearance of infection. We found that hemozoin is more concentrated in the liver at days 0-4 post treatment, after which hemozoin is more concentrated in the spleen. This corresponds to an increase in whole blood concentration during days 4-10 post treatment, suggesting that hemozoin is transported from the liver to the spleen via whole blood during clearance of infection. We were able to quantify hemozoin in both the RBC and plasma fractions of mouse whole blood. We observed a higher hemozoin concentration in RBCs during the first 2 days post clearance. After day 7 however, there were more quantifiable plasma samples than RBC samples. With the exception of 1 sample, we were unable to detect hemozoin in either plasma or RBC fraction past day 25 post treatment.

We were also able to detect and quantify hemozoin in the RBC and plasma fractions of infected human patients' whole blood. Although limited in the number of samples, we observed higher hemozoin concentrations in the RBC fraction as compared to the plasma, and a rapid decline in concentrations between days 0-2 post treatment. These observations reflected what occurred in the mouse model. With more human patient samples, we can continue to utilize our sensitive luminescence assay to observe the kinetics of hemozoin during clearance in *Plasmodium* infected human patients.

Advisor: Dr. David Sullivan

Secondary Reader: Dr. Sean Prigge

ACKNOWLEDGMENTS

There are several important people I would like to acknowledge for their contributions to this thesis. First, I would like to thank my advisor, Dr. David Sullivan, for allowing me to join his lab and being an excellent teacher and mentor. From his first malariology lecture describing malaria as a "stealer of dreams" to his references of hemozoin as "black gold" in the lab, he has generously shared his expertise on malaria and hemozoin with me, making me a better student and scientist. I would also like to thank the Sullivan Lab members for creating an environment which was a joy to work in. Thank you to Dr. Tamaki Kobayashi for her knowledgeable feedback on my thesis work, to Dr. Kristin Poti for her advice on assay development and for being a good friend, to Rachel Evans for teaching me how to culture parasites and for her kindness, and to Tori Balta for being a cohort-mate I could share my experiences with. I would also like to acknowledge the rest of my ScM cohort for the support they have provided me with during my two years at JHSPH. I would like to thank the faculty and admin of the department of Molecular Microbiology and Immunology for providing me with the incredible opportunity to pursue my ScM and for their guidance during this process. In particular, I would like to acknowledge Dr. Sean Prigge for being my secondary reader and thank him for his useful feedback on my thesis.

Finally, I would like to thank my family for their unwavering support of my professional goals. My father, Azhar Sayeed, and my mother, Sameena Kausar, have taught me the importance of ambition, hard work, and determination to achieve the best quality of work, without which I would not have been able to complete this thesis and be the person I am today.

TABLE OF CONTENTS

LIST OF TABLES

LIST OF FIGURES

CHAPTER 1

INTRODUCTION TO HEMOZOIN

INTRODUCTION

Malaria is a life-threatening disease for which roughly half of the world's population is at risk. In 2017, there were an estimated 219 million cases of malaria and 435,000 deaths reported. Over 90% of cases are found in sub-Saharan Africa. High risk populations for malaria include pregnant women and children, where over two-thirds of malaria deaths occur in children under the age 5 [1].

Malaria is the clinical manifestation of infection by the *Plasmodium* parasite. The parasite undergoes a complex life cycle in which asexual replication occurs within host red blood cells (RBCs). Within host RBCs, the parasite degrades hemoglobin for amino acids, a process essential for parasite survival and replication. The heme byproduct is crystalized into hemozoin to remove heme from solution chemistry participating in oxidative-reduction reactions. A single parasite produces ~1.5 fmol of hemozoin during one growth cycle [2]. One human patient with a 1% parasitemia will have $2.4x10^{11}$ parasites in their total 6 L volume of whole blood. Therefore, a single patient will produce $3.6x10^{11}$ fmol of hemozoin. Assuming each of the 217 million cases diagnosed in 2017 had at least a 1% parasitemia, this would yield roughly 48,000 moles of hemozoin or thirty thousand kilograms of heme (616 g/mol) produced from malaria infections in 2017.

Because hemozoin production is an essential part of the *Plasmodium* life cycle, this process is a common drug target for current antimalarials. However, with emerging drug resistance, it is important to elucidate the mechanisms of hemozoin production in order to understand *Plasmodium* responses under drug pressure. In this thesis, we seek to understand parasite stress response by observing the morphological effect of drug

resistance on hemozoin morphology. The chemical and physical properties of hemozoin can be exploited to improve upon detection and diagnosis of malaria. Therefore, in this thesis we also explore the kinetics of hemozoin in blood throughout the clearance of *Plasmodium falciparum* infection in human patients and *Plasmodium berghei* infection in a mouse model.

1.1 The asexual life cycle of *Plasmodium*

The malaria parasite *Plasmodium* has a complex life cycle which requires at least two hosts for it to successfully propagate within a population, attributing to its widespread disease burden. Transmission of the parasite occurs via the female *Anopheles* mosquito. Human infection begins when an infected mosquito takes a bloodmeal from a naïve human while depositing *Plasmodium* sporozoites through its saliva into the dermis. From the skin, the sporozoites use gliding motility to migrate towards blood vessels [3]. Upon entering the bloodstream, the sporozoites traverse to the liver to invade hepatocytes and develop into schizonts. After establishing liver-stage infection over roughly 7-10 days, merosomes bud from the infected hepatocyte to release merozoites into the blood stream [3]. Thus begins the erythrocytic, asexual stages of the parasite life cycle. Upon RBC invasion, the parasite begins its 48 hour intra-erythrocytic life cycle by developing into a ring structure and beginning to feed on the RBC cytoplasm [3,4]. It then matures into a trophozoite, a stage in which hemozoin is detected microscopically, increasing its metabolic activity and restructuring the host RBC. Schizogony occurs as repetitive nuclear division produces around 20 daughter merozoites which are released from the RBC to further invade naïve RBCs. This asexual cycle of invasion, replication, and release during the blood stage of infection allows parasite titers to increase to a level

within the blood that causes the cyclical fevers typically associated with the symptoms of malaria.

During asexual replication within the RBC, a small portion of parasites commit to sexual development to produce male and female gametocytes, also containing hemozoin. Gametocytes sequester in the bone marrow for 11 days to fully mature before they emerge into the peripheral circulation of the now infective human host [3]. *Plasmodium* transmission is driven as mosquitoes become infected when picking up gametocytes from a vertebrate host during a blood meal. Within the mosquito, the parasite develops from a gametocyte in the blood meal to an ookinete, which can traverse the midgut epithelium to form an oocyst on the basal lamina of the mosquito midgut. The oocyst, the final hemozoin-containing stage, harbors development of motile sporozoites, which upon release from the oocyst into the mosquito hemocoel, travel to the salivary glands [5]. Once the salivary glands have been invaded with sporozoites, the mosquito is ready to infect a naïve vertebrate host with *Plasmodium*, continuing the parasite's life cycle and the transmission of malaria.

1.2 Hemoglobin metabolism

During the erythrocytic stages of the *Plasmodium* life cycle, the parasite feeds on host RBC cytoplasm. More than 95% of RBC cytoplasm consists of hemoglobin, of which 60-80% is degraded by the parasite as it matures within the RBC [6]. Amino acids derived from hemoglobin metabolism are essential for parasite survival due to its limited ability for amino acid synthesis or uptake [7]. By inhibiting hemoglobin proteases within the parasite, it has been shown that parasite development is interrupted; therefore, hemoglobin metabolism is an important process for parasite maturation [6]. During early

ring stages, parasite cytostomes pick up small portions of host cytoplasm through micropinocytosis. As the parasite matures into the trophozoite stages, larger volumes of cytoplasm are ingested into vesicles which fuse to form a digestive vacuole within the parasite [6]. This organelle has an estimated pH of 5.0-5.4 and is maintained by a proton gradient which can activate an ATPase pump [8]. The process of hemoglobin degradation within the digestive vacuole is ordered and primarily conducted by aspartic and cysteine proteases. Aspartic protease plasmepsin I is synthesized during early ring stages but is not as abundant as plasmepsin II, which only appears during trophozoite stages [6]. This coincides with the observations that hemoglobin metabolism begins during the ring stage, but an increase in metabolic activity is attributed to trophozoites when most of the host cell cytoplasm is consumed. Plasmepsins I and II initially cleave hemoglobin at the highly specific 33Phe-34Leu site, unraveling the tetramer and allowing for further cleavage at other sites [9,10]. Inhibiting plasmepsin I activity blocks hemoglobin degradation and is lethal to the parasite, whereas plasmepsin II does not seem to be an essential protease for parasite survival [6]. A cysteine protease, falcipain, acts on hemoglobin after it has been denatured by plasmepsins. Blocking cysteine protease activity is detrimental to the parasite as it impairs parasite growth [6]. Figure 1.1 summarizes the predicted pathway of hemoglobin metabolism to produce amino acids for the parasite's use.

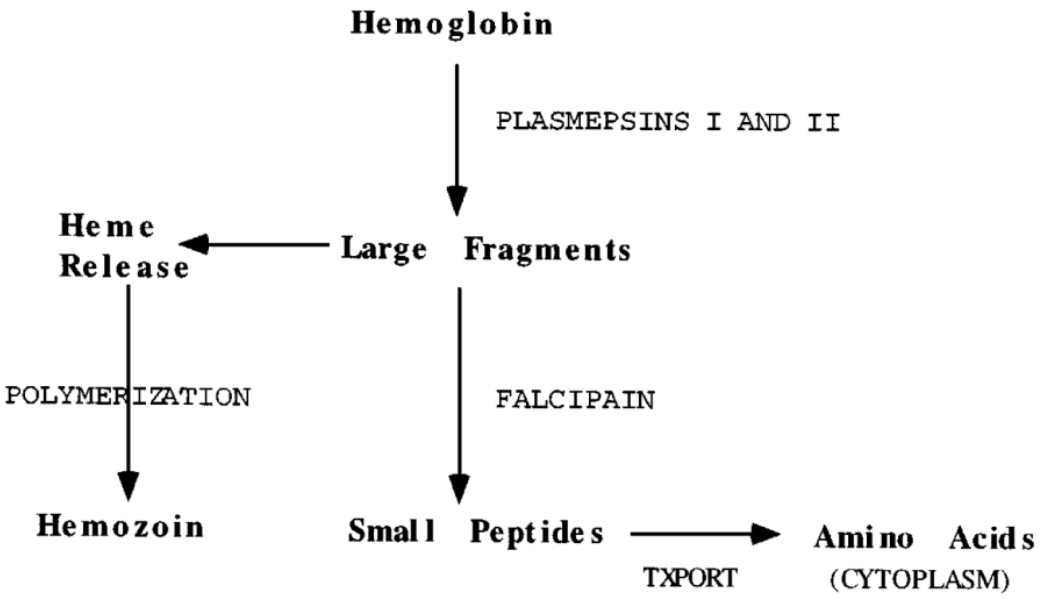

Fig. 1.1 Proposed pathway for hemoglobin degradation in *P. falciparum.*
Taken from Francis et al. [6]

During the process of hemoglobin degradation, free heme is released in the digestive vacuole and oxidized to the ferric state. This oxidation leads to the production of reactive oxygen species such as superoxide anions (O_2^-), hydroxyl radicals ($OH^\bullet$), and hydrogen peroxide (H_2O_2) [6,11]. Oxidative stress caused by reactive oxygen species can damage the parasite digestive vacuole as well as the host cell. Detoxification of heme is required by the parasite due its lack of heme oxygenase as to avoid oxidative stress [12]. Therefore, the parasite sequesters the free heme released from hemoglobin degradation and converts it to an inert crystal in the form of hemozoin [6,12].

1.3 Hemozoin formation

Although the mechanisms of hemozoin formation have not been completely elucidated, several hypotheses have been proposed and disputed. Originally, Slater et al. proposed that hemozoin was a polymer formed by a "heme polymerase" enzyme by demonstrating that monomeric heme polymerization was dependent on time, heat, and

pH [13]. However, the theory of a parasitic enzyme responsible for hemozoin formation was later disproved after lack of deactivation by boiling or adding protease was observed, therefore concluding that the process was autocatalytic in the presence of hemozoin or β-hematin [14]. Additionally, Sullivan et al. proposed that histidine-rich protein II (HRPII) may also be responsible for hemozoin formation [15]. However, later studies showed that clones lacking HRPII genes are still able to produce hemozoin, therefore establishing that HRP is sufficient but not necessary for hemozoin formation [16,17]. Another protein, heme detoxification protein (HDP), has been proposed as being involved in hemozoin production due to its higher heme binding affinity than HRPII [18]. Other studies suggested the theory of neutral lipids associated with the digestive vacuole promoting hemozoin formation [19]. TEM imaging of parasites and subcellular fractionation have identified neutral lipid bodies in association with hemozoin in the digestive vacuole [20]. There is increasing evidence that these digestive vacuole neutral lipid nanospheres accumulate free heme and promote hemozoin formation. Further research is being conducted to identify the necessary conditions for hemozoin formation.

1.4 Hemozoin structure and properties

Early studies on the structure of hemozoin were conducted in 1987 by Fitch and Kanjananggulpan who purified hemozoin and studied its solubility properties to show it consisted of ferriprotoporphyrin IX (Fe(III)PPIX), an iron atom surrounded by a porphyrin ring structure of four nitrogen atoms, suggesting this structure to be identical to β-hematin, a synthetic Fe(III)PPIX [12,21]. This was confirmed with X-ray diffraction patterns showing that the chemical structure of hemozoin is indeed identical to that of β-hematin [22,23]. In 2000, when the structure of β-hematin was deduced, early

assumptions of hemozoin as a polymer were invalidated. We now know that hemozoin is a crystalline dimer with iron carboxylate bonds to the propionic side chains of the porphyrin ring [24]. Hemozoin crystals from mammalian *Plasmodium* are brick-like structures with an average dimension of 100 nm x 100n m x 300-500 nm [25]. When compared to hemozoin from other *Plasmodium* species, hemozoin morphology can differ by shape and size [25].

Because the structure of hemozoin is similar to that of β-hematin as was shown by similar IR spectra and X-ray diffraction, certain properties of β-hematin reflect those of hemozoin. For example, hematin has paramagnetic properties that can be exploited to develop hemozoin detection or quantification tools. This property has been previously used for separating infected RBCs from uninfected RBCs. The unique optical dichroism patterns generated from the crystal structure of hematin can be combined with its magnetic properties to develop diagnostic tools. It has also been observed that exposure of a parasite to a strong magnetic field can spin hemozoin crystals and potentially disrupt hemozoin formation [12]

1.5 Malaria diagnostics and hemozoin as a biomarker

An essential component of eliminating malaria worldwide is accurate diagnosis of the disease. Due to its nonspecific clinical presentation such as fever and other flu-like symptoms, misdiagnosis is possible and can have serious consequences. Nonetheless, clinical diagnosis of malaria is commonly used in endemic regions where there is lack of access to other diagnostic tools. The current gold standard for malaria diagnosis is microscopy. This involves taking a peripheral blood sample to make a blood film on which parasites are visualized by Giemsa staining. This method is quick and reliable, and

is currently the most efficient way to make a malaria diagnosis in the field. However, microscopy has a limit of detection of 50-100 parasites/ul, which is a disadvantage when trying to detect subclinical malaria in which low parasite burden exists but does not cause clinical symptoms [26]. Therefore, molecular diagnostics, such as detecting parasite DNA or RNA using PCR, are a more sensitive method to accurately confirm infection. Because the limit of detection for PCR is 0.5-1 parasite/ul, subclinical malaria can also be diagnosed [26]. However, PCR is not a practical tool to use in the field due to limiting requirements of having an extensive lab setting with trained professionals to perform the assay. A third major class of malaria diagnostics includes rapid detection tests (RDTs). Although not quantitative like microscopy or PCR, RDTs are simple to use making them an excellent candidate for field diagnostics. They only require 10-15ul of blood and results are obtained immediately. RDTs rely on parasitic antigens such as aldolase or HRPII as a method of detection [26]. However, there is evidence that these antigens can linger in peripheral blood after clearance of infection, therefore increasing the possibility of false positives by RDT [27]. There is a continuous push to increase the sensitivity of the current diagnostic tools used in the field without compromising the accuracy of the diagnosis.

Other innovative methods are being explored to detect malaria infection. This includes utilizing the properties of hemozoin to create diagnostic tools. The diverse properties of hemozoin allow it to be detected in several different ways. The most explored method of hemozoin detection is by using mass spectrometry to identify the ionized fragments of heme crystals. Specifically using laser-desorption mass spectrometry (LDMS) excitation of hemozoin heme produces ions which acquire kinetic

energy proportional to their charge. Ions with different masses have different times-of-flight (TOF) which are recorded in a spectrum [28]. The parent fragment used to identify hemozoin occurs at a unique mass to charge ratio of 616 m/z (the molecular weight of heme is 616 Da), with other characteristic fragments occurring at 484, 498, 512, 526, 557, and 571 m/z [28]. Studies have shown successful detection of hemozoin using LDMS both *in vitro* and *in vivo*. Non-invasive methods exploiting the excitation properties of hemozoin heme are being explored as diagnostic tools [29]. However, creating a portable and affordable device to detect hemozoin using mass spec has yet to be accomplished.

The magnetic and birefringent properties of hemozoin are also being used to develop novel diagnostic tools to use in the field. Such devices use a magnet to align hemozoin such that the crystals block polarized light. The amount of light blocked is proportional to the concentration of hemozoin [30]. The sensitivity of magneto-optical hemozoin diagnostic tools is 10-40 parasites/ul [29]. This avenue of diagnosis is comparatively more sensitive than microscopy diagnosis but still not as sensitive as nucleic acid detection. Another diagnostic technique being developed uses laser pulses to create hemozoin-generated vapor nanobubbles underneath the skin, avoiding the use of a needle to obtain blood [31]. Therefore, there are a variety of methods being explored using hemozoin as a diagnostic tool.

1.6 Kinetics of hemozoin formation

Up to 95% of heme iron released from hemoglobin degradation is sequestered to form hemozoin within the *Plasmodium* digestive vacuole [32]. This was observed by measuring the total iron in parasitized RBCs, isolated trophozoites, and digestive

vacuoles. Parasitized RBCs contain the same amount of iron as non-parasitized cells: ~90-111 fg/cell, indicating that there is no significant loss of iron during parasitic invasion of an erythrocyte [32]. Mössbauer spectroscopy of trophozoites only identified spectra of iron species identical to that of β-hematin. Because hemozoin has an identical structure to synthetic β-hematin, researchers concluded that hemozoin is the only detectable iron species within a trophozoite. These observations were further verified using microscopy, in which the distribution of iron within a trophozoite-infected RBC overlapped with hemozoin within the parasite and was devoid from the erythrocytic cytosol [32]. Another study used spinning disk confocal microscopy to acquire live 3D images of intraerythrocytic parasites. Using this technique researchers were able to measure the kinetics of hemozoin formation, observing the production of 1.5 fmols of hemozoin per parasite at the end its trophozoite stage [2].

Quantification of hemozoin from parasites in synchronized cultures shows low levels of production at early ring stages within the host RBC. Hemozoin noticeably appears at 15-19 hours post synchronization to rings. Production rapidly increases between 25-30 hours post synchronization, aligning with the time of trophozoite development and increased hemoglobin metabolism. Post hour 30, hemozoin levels plateau off [2]. After RBC lysis, hemozoin is released into circulation and can be picked up by phagocytes. Hemozoin crystals picked up by macrophages are toxic to these cells and can permanently damage and deplete their functionality. Other immunomodulatory effects of hemozoin have also been explored, such as the production of inflammatory cytokines and the inhibition of erythropoiesis leading to anemia and other malaria pathology [12].

1.7 Blood stage antimalarials

The use of antimalarials dates back to the 1600s with the discovery of a Cinchona bark extract known as quinine. It was from this natural remedy that future antimalarial drugs such as the widely used chloroquine were derived [33]. Chloroquine belongs to a larger class of antimalarials known as 4-aminoquinolines. This class includes other potent antimalarials such as piperaquine, amodiaquine, and pyronaridine [34]. Chloroquine is a weak base allowing it to easily permeate membranes, making its way into the acidic environment of the parasite digestive vacuole. Once protonated in the acidic digestive vacuole, chloroquine is unable to diffuse back out and therefore accumulates to lethal levels within the parasite [17]. It has been shown that chloroquine interaction with hematin inhibits crystal growth [35]. Because the conversion of toxic free heme to hemozoin is essential for parasite survival, disrupting this process with chloroquine is lethal to the parasite. This mechanism of action also applies to other potent 4-aminoquinolines. It is therefore understandable that 4-aminoquinolines are most potent against the erythrocytic stages of the parasite life cycle.

Chloroquine was deployed to treat malaria worldwide in the 1900s and was largely successful until resistance against the drug emerged in the 1960s. Chloroquine resistance was attributed to a single point mutation in the *Pf*CRT gene coding for the chloroquine resistant transporter protein responsible for exporting protonated chloroquine from the digestive vacuole, preventing it from accumulating to high enough concentrations to be effective against the parasite [33]. Resistance to the most widely used antimalarial was devastating to the fight against malaria and therefore pushed researchers to seek alternative treatments. This eventually led to the discovery of

artemisinin, derived a Chinese medicinal drug known as *qinghao* [33]. Artemisinin and other artemisinin derivatives such as artemether, artesunate, and dihydroartemisinin, are endoperoxides [34]. This class of drugs is activated by free heme which cleaves the endoperoxide bridge to form free radicals within the parasite to rapidly damage bystander proteins [33]. Similar to chloroquine, artemisinins are most effective against blood stage malaria. Because artemisinins must be activated by free heme, they are particularly potent during trophozoite stage where most hemoglobin degradation is occurring and large amounts of free heme are available. Unlike chloroquine, however, artemisinins do not directly bind hemozoin to inhibit its formation. Artemisinins are fast acting drugs with short half-lives and are therefore often paired with longer lasting drugs to create artemisinin combination therapies (ACTs) to ensure full parasite clearance.

More recently, resistance to artemisinin treatment has emerged in Southeast Asia. This is was observed as significantly delayed parasite clearance in patients treated with artesunate in Western Cambodia as compared to patients who received the same treatment across the border in Thailand [36]. Upon genomic analysis of parasite strains isolated from resistant patients, a single point mutation in the Kelch 13 propeller region showed to confer resistance, the most commonly occurring SNP being a cysteine to tyrosine polymorphism at position 580 (C580Y) [37]. Because artemisinins are fast acting drugs, ring-stage assays were developed to measure drug inhibition immediately post invasion as opposed to the traditional IC_{50} which exposes higher concentration of drug for a longer period of time. Ring stage assays of strains with K13 mutations inserted into a wild type Cambodian background demonstrated longer survival of ring stage parasites after exposure to dihydroartemisinin (DHA) [38]. Therefore, the K13 mutation

conferred ring-stage resistance to artemisinin. Further studies showed altered parasite development in mutant strains. Resistant strains exhibited a prolonged ring stage and subsequently shorter trophozoite stage [39]. One hypothesis behind this mechanism could be that the parasites have adapted to reduce the amount of free heme exposed to artemisinin during hemoglobin degradation by reducing the amount of time spent in the trophozoite stage.

REFERENCES

1. Malaria [Internet]. [cited 2019 Mar 9]. Available from: https://www.who.int/news-room/fact-sheets/detail/malaria

2. Gligorijevic B, McAllister R, Urbach JS, Roepe PD. Spinning disk confocal microscopy of live, intraerythrocytic malarial parasites. 1. Quantification of hemozoin development for drug sensitive versus resistant malaria. Biochemistry [Internet]. UTC; 2006 [cited 2019 Mar 6];45:12400–10. Available from: https://pubs.acs.org/sharingguidelines

3. Cowman AF, Healer J, Marapana D, Marsh K. Malaria: biology and disease. Cell [Internet]. Elsevier Inc.; 2016;167:610–24. Available from: http://dx.doi.org/10.1016/j.cell.2016.07.055

4. Bannister LH, Hopkins JM, Fowler RE, Krishna S, Mitchell GH. A brief illustrated guide to the ultrastructure of *Plasmodium falciparum* asexual blood stages. Parasitol Today. 2000;16:427–33.

5. Aly ASI, Vaughan AM, Kappe SHI. Malaria parasite development in the mosquito and infection of the mammalian host. Annu Rev Microbiol. 2009;63:195–221.

6. Francis SE, Sullivan DJ, Goldberg and DE. Hemoglobin metabolism in the malaria parasite *Plasmodium falciparum*. Annu Rev Microbiol. 2002;51:97–123.

7. Sherman IW. Amino acid metabolism and protein synthesis in malarial parasites. Bull World Health Organ [Internet]. World Health Organization; 1977 [cited 2019 Feb 20];55:265–76. Available from: http://www.ncbi.nlm.nih.gov/pubmed/338183

8. Krogstad DJ, Schlesinger PH, Gluzman IY. Antimalarials increase vesicle pH in *Plasmodium falciparum*. J Cell Biol [Internet]. 1985 [cited 2019 Feb 20];101:2302–9.

Available from: http://doi.org/10.1083/jcb.101.6.2302

9. Gluzman Y, Francis SE, Oksman A, Smith CE, Duffin KL, Goldberg DE. Order and specificity of the *Plasmodium falciparum* hemoglobin degradation pathway. J Clin Invest [Internet]. 1994 [cited 2019 Feb 20];93:1602–8. Available from: https://www-ncbi-nlm-nih-gov.proxy1.library.jhu.edu/pmc/articles/PMC294190/pdf/jcinvest00033-0264.pdf

10. Goldberg DE, Slater AFG, Beavis R, Chait B, Cerami A, Henderson GB. Hemoglobin degradation in the human malaria pathogen *Plasmodium falciparum* : A catabolic pathway initiated by a specific aspartic protease. [cited 2019 Feb 20]; Available from: http://doi.org/10.1084/jem.173.4.961

11. Atamna H, Ginsburg H. Origin of reactive oxygen species in erythrocytes infected with *Plasmodium falciparum*. Mol Biochem Parasitol [Internet]. 1993 [cited 2019 Feb 20];61:231–41. Available from: http://www.ncbi.nlm.nih.gov/pubmed/8264727

12. Coronado LM, Nadovich CT, Spadafora C. Malarial hemozoin: From target to tool. Biochim Biophys Acta - Gen Subj [Internet]. Elsevier B.V.; 2014;1840:2032–41. Available from: http://dx.doi.org/10.1016/j.bbagen.2014.02.009

13. Slater AFG, Cerami A. Inhibition by chloroquine of a novel haem polymerase enzyme activity in malaria trophozoites. Nature. 1992;355:167–9.

14. Dorn A, Stoffel R, Matile H, Bubendorf A, Ridley RG, Malarial Haemozoin. Malarial haemozoin/b-hematin supports haem polymerization in the absence of protein. Nature. 1995;374:271.

15. Sullivan Jr DJ, Gluzman IY, Goldberg DE. *Plasmodium* hemozoin formation mediated by histidine-rich proteins. 2017;271:219–22.

16. Egan TJ. Recent advances in understanding the mechanism of hemozoin (malaria

pigment) formation. J Inorg Biochem. 2008;102:1288–99.

17. Sullivan DJ. Theories on malarial pigment formation and quinoline action. Int J Parasitol. 2002;32:1645–53.

18. Jani D, Nagarkatti R, Beatty W, Angel R, Slebodnick C, Andersen J, et al. HDP - A novel heme detoxification protein from the malaria parasite. PLoS Pathog. 2008;4.

19. Bendrat K, Berger BJ, Cerami A. Haem polymerization in malaria. Nature. 1995;378:138.

20. Pisciotta JM, Coppens I, Tripathi AK, Scholl PF, Shuman J, Shulaev V, et al. The role of neutral lipid nanospheres in *Plasmodium falciparum* haem crystallization. Biochem J. 2007;402:197–204.

21. Fitch CD, Kanjananggulpan P. The state of ferriprotoporphyrin IX in malaria pigment. J Biol Chem [Internet]. 1987;262:15552–5. Available from: http://www.jbc.org/content/262/32/15552.full.pdf

22. Slater AF, Swiggard WJ, Orton BR, Flitter WD, Goldberg DE, Cerami A, et al. An iron-carboxylate bond links the heme units of malaria pigment. Proc Natl Acad Sci. 2006;88:325–9.

23. Bohle DS, Dinnebier RE, Madsen SK, Stephens PW. Characterization of the products of the heme detoxification pathway in malarial late trophozoites by X-ray diffraction. J Biol Chem. 1997;272:713–6.

24. Pagola S, Stephens PW, Bohle DS, Kosar AD, Madsen SK. Structure of malaria pigment b-Haematin. Nature. 2000;404:307–10.

25. Noland GS, Briones N, Sullivan DJ. The shape and size of hemozoin crystals distinguishes diverse *Plasmodium* species. Mol Biochem Parasitol. 2003;130:91–9.

26. Tangpukdee N, Duangdee C, Wilairatana P, Krudsood S. Malaria diagnosis: A brief review. Korean J Parasitol. 2009;47:93–102.

27. Mayxay M, Pukrittayakamee S, Chotivanich K, Looareesuwan S, White NJ. Persistence of *Plasmodium falciparum* HRP-2 in successfully treated acute falciparum malaria. Trans R Soc Trop Med Hyg. 2004;95:179–82.

28. Demirev PA. Mass spectrometry for malaria diagnosis. Expert Rev Mol Diagn. 2004;4:821–9.

29. Zimmerman PA, Howes RE. Malaria diagnosis for malaria elimination. Curr Opin Infect Dis. 2015;28:446–54.

30. Grimberg BT, Grimberg KO. Hemozoin detection may provide an inexpensive, sensitive, 1-minute malaria test that could revolutionize malaria screening. Expert Rev Anti Infect Ther. 2016;14:879–83.

31. Campbell KM, Braam J, Ware RE, Sullivan DJ, Lukianova-Hleb EY, Olson JS, et al. Hemozoin-generated vapor nanobubbles for transdermal reagent- and needle-free detection of malaria. Proc Natl Acad Sci. 2013;111:900–5.

32. Egan TJ, Taylor D, Egan J, Smith PJ, Walden JC, Marques HM, et al. Fate of haem iron in the malaria parasite *Plasmodium falciparum*. Biochem J. 2002;365:343–7.

33. Fong KY, Wright DW. Hemozoin and antimalarial drug discovery. Future Med Chem. 2013;5:1437–50.

34. Sinden RE, Plouffe D, Meister S, Scheurer C, Delves M, Wittlin S, et al. The activities of current antimalarial drugs on the life cycle stages of *Plasmodium*: A comparative study with human and rodent parasites. PLoS Med. 2012;9:e1001169.

35. Gorka AP, Alumasa JN, Sherlach KS, Jacobs LM, Nickley KB, Brower JP, et al.

Cytostatic versus cytocidal activities of chloroquine analogues and inhibition of hemozoin crystal growth. Antimicrob Agents Chemother. 2013;57:356–64.

36. Dondorp AM, Nosten F, Yi P, Das D, Phyo AP, Tarning J, et al. Artemisinin resistance in *Plasmodium falciparum* malaria. N Engl J Med. 2009;365:455–67.

37. Ariey F, Witkowski B, Amaratunga C, Beghain J, Langlois AC, Khim N, et al. A molecular marker of artemisinin-resistant *Plasmodium falciparum* malaria. Nature. 2014;505:50–5.

38. Straimer J, Gnadig NF, Witkowski B, Amaratunga C, Duru V, Ramadani AP, et al. K13-Propeller mutations confer artemisinin resistance in *Plasmodium falciparum* clinical isolates. Science (80-). 2015;347:428–31.

39. Hott A, Casandra D, Sparks KN, Morton LC, Castanares GG, Rutter A, et al. Artemisinin-resistant *Plasmodium falciparum* parasites exhibit altered patterns of development in infected erythrocytes. Antimicrob Agents Chemother. 2015;59:3156–67.

CHAPTER 2

ANALYZING THE MORPHOLOGY OF HEMOZOIN IN DRUG RESISTANT *PLASMODIUM*

INTRODUCTION

Artemisinin (ART) derivatives are fast-killing antimalarials that are currently the gold standard treatment against malaria. Therefore, development of ART resistance is of great concern, especially due to emerging evidence of this occurrence in Southeast Asia over the last several years. Artemisinins, as with other common classes of antimalarials, target the erythrocytic stages of the *Plasmodium* life cycle. As the parasite digests host red blood cell (RBC) hemoglobin within the acidic environment of its digestive vacuole, it releases toxic heme in the form of reduced iron (Fe^{2+}). Heme activates ART by cleaving its endoperoxide bridge. ART radicals, derived from activation, damage surrounding proteins and effectively kill the parasite [1,2]. Because hemoglobin metabolism begins in the ring stage and largely occurs during the trophozoite stage, ARTs are effective in rapidly killing blood stage parasites: they can reduce parasite burden by 10,000-fold every 48 hours [3]. However, stage and time-dependence of ART killing is an important factor to consider when administering ART based treatment. Because ART has a short half-life (~1 hour in humans) and ring-stage parasites are less susceptible to ART killing, combination therapies are required to ensure true clearance of parasites. Therefore, ART-based combination therapies (ACTs) employ a partner drug [ex. mefloquine, piperaquine, lumefantrine] with a longer half-life that can eliminate residual parasites and prevent recrudescence [1,4].

In 2009, Dondorp et al. reported prolonged parasite clearance in patients treated with artesunate in Western Cambodia [4]. Specifically in the Pailin region of Western Cambodia, median parasite clearance was reported to be 84 hours as compared to 48 hours in the Wang-Pha region of nearby Thailand, depicted in Fig. 2.1 [4].

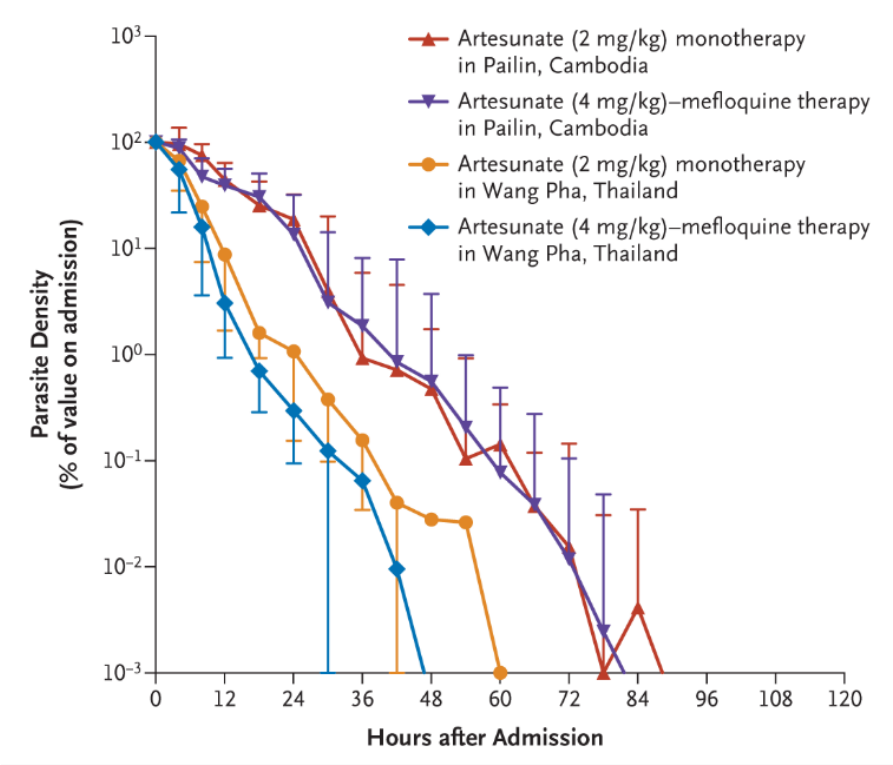

Fig. 2.1 Parasite clearance curves.
Taken from Dondorp et al. [4]

To further explore this reduced susceptibility to ARTs, Witkowski et al. developed a novel "ring-stage assay" (RSA) to measure drug susceptibility 0-3 hours post-invasion as opposed to a traditional IC50 assay in which parasites are exposed to high concentrations of drug for 48-72 hours Using the RSA0-3h, they were able to successfully identify slow-clearing infections in Pursat, Cambodia. Rings cultured from these infections showed higher survival rates and therefore reduced susceptibility to a 6 hour exposure to 700 nM dihydroartemisinin [5]. Genome wide- association studies were performed to identify the genetic drivers for ring stage resistance to ARTs. Ariey et al. observed four SNPs within a Kelch repeat of the K13 propeller domain: Y493H, R539T, I543T, and C580Y, which associate with higher RSA0-3h survival rates [6]. Additionally, K-13 mutants clustered within areas of Cambodia in which delayed

clearance to ARTs was clinically observed [6]. These studies established specific K13 polymorphisms as genetic markers of decreased ART susceptibility in western Cambodia.

Further studies involving genetic manipulation of culture-adapted Cambodian isolates revealed lower ring-stage survival after exposure to DHA upon removal of K13 SNPs I543T and C580Y. The mutations were also introduced into fast-clearing wild type isolates and an increase in RSA0-3h survival was subsequently observed [7]. These studies further verified the causal role of K13 SNPs in conferring ring-stage artemisinin resistance. However, the molecular mechanisms of this phenomenon have not been completely elucidated. Transcriptomic studies by Mok et al. revealed decelerated development of resistant parasites and upregulation within a protein pathway involving *Plasmodium* reactive oxidative stress complex (PROSC) and TCP-1 ring complex (TRiC) [8]. Altered intraerythrocytic development in resistant parasites from Cambodian clinical isolates was also observed by Hott et al [9]. Morphological observations revealed a prolonged ring stage and compressed trophozoite stage as schizogony was completed simultaneously to an artemisinin susceptible strain. The ring-stage in resistant parasites lasted up to 14 hours longer (30 hours total) than the control [9]. Because the parasite life cycles were synchronized and schizogony occurred simultaneously, time for trophozoite development in resistant parasites was shortened. Hott et al. hypothesize that perhaps parasites have evolved to reduce ART exposure to the trophozoite stage. After all, increased metabolism during trophozoite stages releases the free heme needed to activate ART drugs. Therefore, by reducing heme exposure to ART, the parasite is potentially able to avoid damage caused by activated ART.

Antimalarials such as the 4-aminoquinolines target hemozoin production by inhibiting crystal growth allowing for the accumulation of toxic free heme within the parasite digestive vacuole [10]. As previously discussed, artemisinins are activated by free heme to form damaging radicals. Therefore, the hemoglobin digestion and hemozoin formation pathway are prime targets for antimalarials. If the parasite alters this process, it could potentially attenuate the efficacy of antimalarials. *Plasmodium* has evolved to confer resistance to previous and current antimalarials by developing ways to avoid or overcome drug pressure. These parasite stress responses remain to be elucidated. In this project, we aim to consider altered hemozoin production as a possible stress response to confer resistance. We asked whether drug resistant *Plasmodium falciparum* strains with compressed trophozoite stages produce hemozoin with altered morphology. We hypothesized that altered development of parasites due to drug resistance would effect hemozoin production and therefore produce crystals of altered shape or size as compared to drug sensitive parasites.

METHODS

Sources of hemozoin

P. falciparum strains CamWT and C580Y were maintained in culture at 2% hematocrit in RPMI 1640 media supplemented with L-glutamine, 25mM HEPES, 0.25% $NaHCO_3$, 0.37 mM hypoxanthine, 50 ul of 50 mg/ml gentamycin, and 10% human serum. Cultures were incubated at 37°C in 5% CO_2/5% O_2/Balanced N_2. *P. falciparum* cultures were synchronized to ring stage by incubation in 5% sorbitol. Parasitemia was assessed by light microscopy of a Giemsa-stained blood film. Trophozoites were isolated by saponin lysis and pelleted to be stored at -80°C until processed for purifying hemozoin. Purified hemozoin for FCR3 and ITG were provided by Dr. David Sullivan for FEISEM images. FEISEM images of previously imaged strains 3BD, 3D7, D10, FCB, 106/1, and *P. berghei* NYU-2 were provided by Dr. David Sullivan for analysis.

Hemozoin purification

Pellets from saponin lysed cultures were thawed at room temperature before processing. Each pellet was washed by adding 1 ml 2% sodium dodecyl sulfate (SDS), then briefly sonicated, followed by centrifugation at 13000 rpm for 5 mins. The supernatant was removed and discarded and the SDS wash was repeated. After 2x SDS washes, 1 ml of proteinase K (Invitrogen cat no. 25530-031, 1 mg/ml in proteinase K buffer solution of 10 mM TrisHCl, 0.5% SDS, and 1 mM $CaCl_2$) was added to each sample, vortexed, and then incubated in a 56°C water bath overnight. The following day, the samples were removed from the water bath and centrifuged at 13000 rpm for 5 mins. Once the supernatant was removed, 2x more SDS washes were performed using the same method as mentioned. Following the SDS washes, a water wash was performed by

adding 1 ml water to each pellet, sonicating, centrifuging at 13000 rpm for 7 mins, and discarding the supernatant very carefully. Water washes were performed until the supernatant looked clear with a visible pellet remaining. A maximum of 6x water washes were performed. After the final wash, the purified hemozoin pellet was resuspended by sonication in 1ml water.

Hemozoin quantification

The purified hemozoin samples were briefly sonicated before quantification. Each sample was plated at 10 ul, 20 ul, and 30 ul in a clear, flat-bottom 96-well plate. The samples were de-crystallized in the 96-well plate by adding 2% SDS/50mM NaOH (pH 9.0) to each well, with a total volume of 200 ul per well. A standard curve was developed by creating a serial dilution of hemin in 2% SDS at concentrations ranging from 10 nmols to 0.1 nmols hemin per well. 100 ul 2% SDS was plated as a negative control. 2%SDS/50mM NaOH was also added to the hemin standard curve and negative control to total 200 ul per well. All samples, as well as the standard curve and negative control were analyzed in duplicate wells. The plate was incubated at room temperature for 30 mins. Successful de-crystallization had occurred if the samples were visibly green in color after incubation. After incubation, the plate was read on the SpectraMax M2 plate reader to measure absorbance at 405 nm. The lower limit of detection was determined to be at an optical density (OD) of 0.2 and saturation occurred at an OD of 2.5. Hemozoin samples were quantified by using a linear regression equation of the hemin standard curve at concentrations between 10 nmol to 1 nmol per well to calculate the concentration of hemozoin per well.

Field Emission In-lens Scanning Electron Microscope (FEISEM) imaging

Hemozoin was coated on silica chips following a previously described protocol [11]. 7-8 nmols hemozoin were coated on each chip. Hemozoin coating was verified using microscopy. After critical point drying, the hemozoin containing chips were coated with gold and imaged on the FIESEM (Leo 1550). About 15 to 20 images were taken per sample.

Hemozoin measurements

The image analysis software ImageJ was used to measure hemozoin dimensions. Images were magnified so that roughly 20 pixels was equivalent to 100nm. The line-drawing tool was used to measure the scale on each image to produce a pixel equivalent value. The line-drawing tool was then used to measure 3 lengths and 3 widths per crystal as depicted in Fig. 2.2. The software automatically converted the measurements to nm, which were then averaged to produce one measurement of length and one measurement of width per crystal.

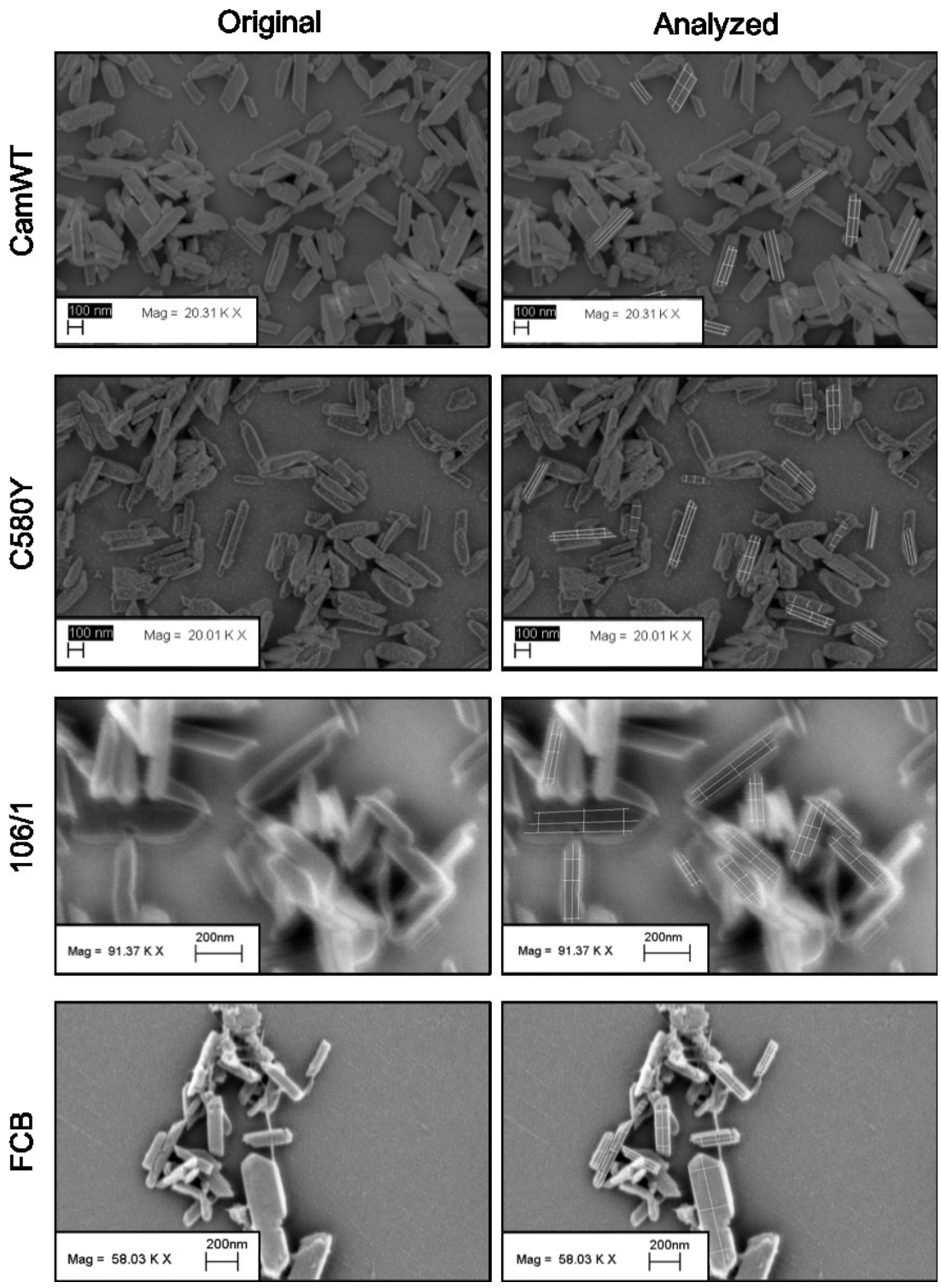

Fig. 2.2 FEISEM images of *Pf* hemozoin and ImageJ analysis.
Representative images taken with FEISEM were analyzed by using ImageJ to draw lines along the lengths and widths of each crystal. Three measures were taken for each crystal length and width: two on each edge and one down the center. The three measures were averaged to obtain a single value for crystal length and width.

Data Analysis

Data was analyzed using GraphPad Prism (v6). Individual crystal measurements were plotted along with the mean ± SEM for each sample. Unpaired t-tests were performed to measure the significance of comparisons between strain dimensions.

RESULTS

Hemozoin in isogenic drug resistant *Plasmodium* is smaller in size

The first two isogenic strains we compared were ring-stage artemisinin sensitive *Pf*CamWT and ring-stage artemisinin resistant *Pf*C580Y which differ by a single Kelch13 point mutation [6,7]. Upon measurement of the lengths and widths of the hemozoin crystals from each strain, C580Y hemozoin crystals were smaller than CamWT, with a statistically significant difference in width between the two strains. Individual and mean ± SEM lengths and widths of CamWT and C580Y hemozoin can be found in Fig. 2.3.

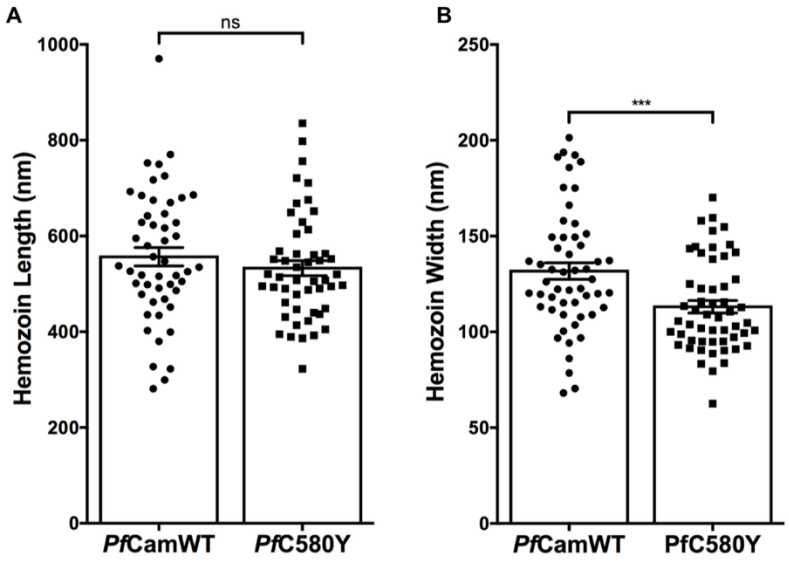

Fig. 2.3 Comparison of hemozoin dimensions of *P. falciparum* strains CamWT and C580Y.
Hemozoin crystal lengths and widths are presented in nm for the isogenic *Pf* strains: ring-stage artemisinin sensitive Cambodian Wild Type (CamWT) and ring-stage artemisinin resistant C580Y. Each point represents the measurement of an individual hemozoin crystal with mean ± SEM displayed. Statistical analysis was conducted using an unpaired t-test to compare length and width measures between strains. (A) Mean hemozoin length was 556.5nm ± 19.2nm for CamWT and 532.8nm ± 15.7nm for C580Y. Statistical analysis resulted in a p-value of 0.341 (ns). N=50 individual crystals were measured for each strain. (B) Mean hemozoin width was 131.7nm ± 4.3nm for CamWT and 113.1nm ± 3.2nm for C580Y. Statistical analysis resulted in a p-value of 0.0008. N=54 individual crystals were measured for each strain.

Chloroquine sensitive (CQS) *Pf*106/1 was compared to chloroquine resistant (CQR) *Pf*FCB. Resistance in *Pf*FCB is conferred by a K76T point mutation in the *Pfcrt* gene, providing us with another comparison of hemozoin dimensions between isogenic *Pf* strains but with different drug susceptibilities [12]. In this case, FCB hemozoin was significantly smaller in both width and length as compared to 106/1 hemozoin as depicted in Fig. 2.4.

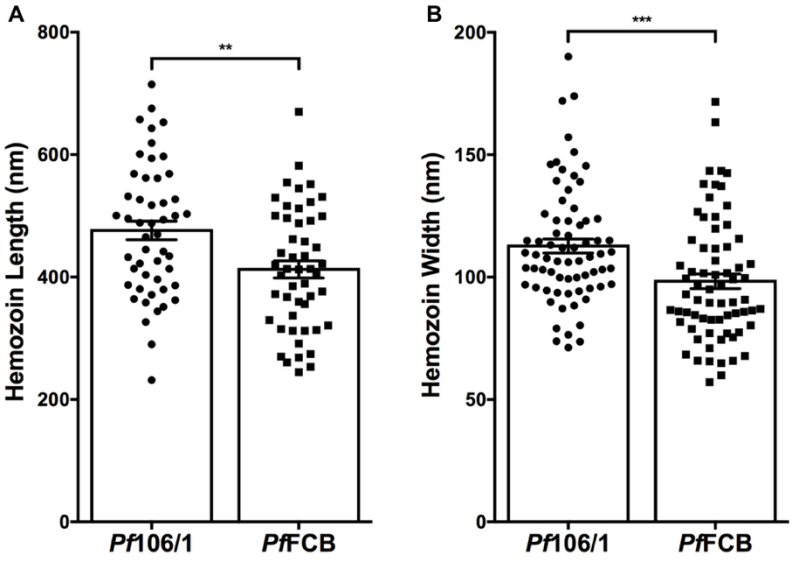

Fig. 2.4 Comparison of hemozoin dimensions of *P. falciparum* strains 106/1 and FCB.
Hemozoin crystal lengths and widths are presented in nm for the isogenic *Pf* strains: chloroquine sensitive 106/1 and chloroquine resistant FCB. Each point represents the measurement of an individual hemozoin crystal with mean ± SEM displayed. Statistical analysis was conducted using an unpaired t-test to compare length and width measures between strains. (A) Mean hemozoin length was 476.1nm ± 15.2nm for 106/1 and 412.6nm ± 14.0nm for FCB. Statistical analysis resulted in a p-value of 0.003. N=50 individual crystals were measured for each strain. (B) Mean hemozoin width was 112.7nm ± 2.9nm for 106/1 and 98.3nm ± 3.0nm for FCB. Statistical analysis resulted in a p-value of 0.0007. N=70 individual crystals were measured for each strain.

A third comparison of hemozoin dimensions between isogenic strains was made with *P. berghei*. CQR *P. berghei* NYU-2 was developed by keeping the CQS parent strain under chloroquine pressure in a mouse model [13,14]. Chloroquine resistance is

reversible and postulated to be transcriptional rather than by SNP because the *PbCRT* gene is unaltered. Hemozoin crystals from the CQR *Pb*NYU-2 strain were also observed to be smaller than the CQS strain, with statistically significant differences in both crystal length and width (Fig. 2.5).

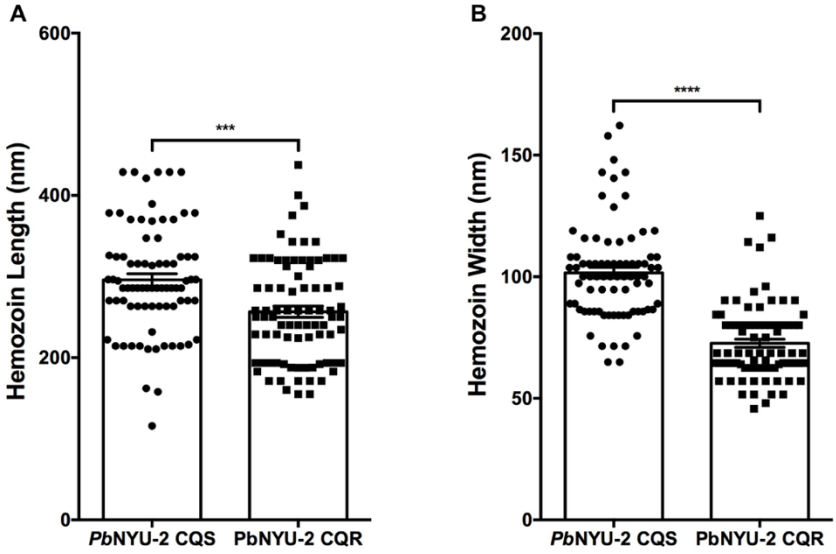

Fig. 2.5 Comparison of hemozoin dimensions of CQS and CQR *P. berghei* NYU-2 strains.
Hemozoin crystal lengths and widths are presented in nm for the isogenic *Pb* strains: CQS *Pb*BYU-2 and CQR *Pb*NYU-2. Each point represents the measurement of an individual hemozoin crystal with mean ± SEM displayed. Statistical analysis was conducted using an unpaired t-test to compare length and width measures between strains. N=79 and n=83 individual crystals were measured for each strain respectively. (A) Mean hemozoin length was 295.8nm ± 7.5nm for CQS *Pb*NYU-2 and 256.6nm ± 6.9nm for CQR *Pb*NYU-2. Statistical analysis resulted in a p-value of 0.0002. (B) Mean hemozoin width was 101.6nm ± 2.2nm for CQS *Pb*BYU-2 and 72.6nm ± 1.7nm for CQR *Pb*NYU-2. Statistical analysis resulted in a p-value of <0.0001.

Hemozoin dimensions of non-isogenic *P. falciparum* strains

Hemozoin dimensions of CQS *Pf* strains NF54, 3D7, and HB3 were compared to those of CQR *Pf* strains ITG, DD2, FCR3 (Fig. 2.6). The CQR strains were not isolated clones of the CQS strains being compared. No significant difference was observed between the lengths nor the widths of crystals in comparisons between each individual

CQS strain to each CQR strain as well as a comparison between mean crystal size of all non-isogenic CQS to CQR strains. Analyzed images of the non-isogenic strains can be found in Fig. 2.7.

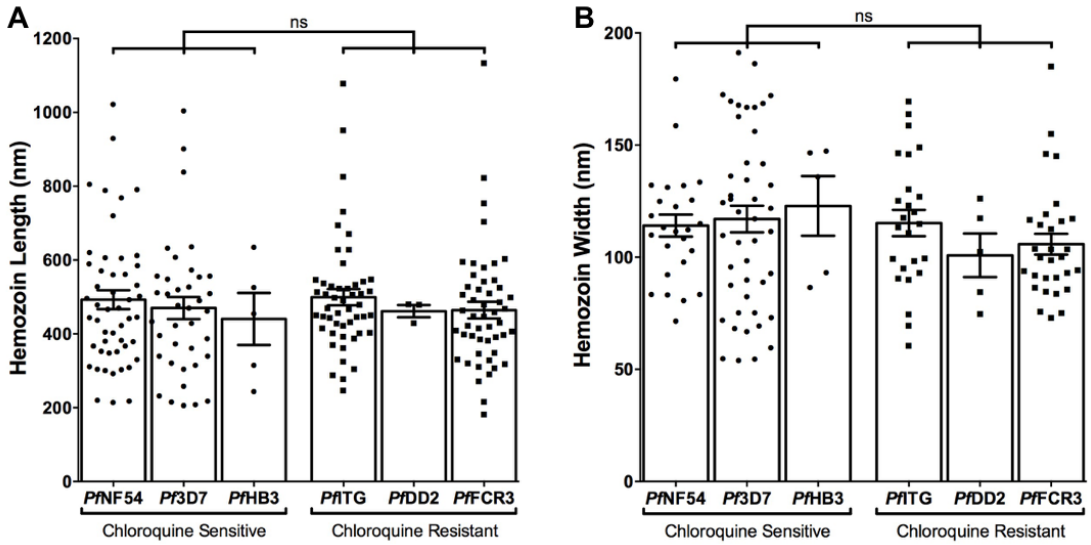

Fig. 2.6 Comparison of hemozoin dimensions of non-isogenic *P. falciparum* strains. Hemozoin crystal lengths and widths are presented in nm for the non-isogenic chloroquine sensitive (CQS) *Pf* strains NF54, 3D7, HB3 and chloroquine resistant (CQR) *Pf* strains ITG, DD2, FCR3. Each point represents the measurement of an individual hemozoin crystal with mean ± SEM displayed. Statistical analysis was conducted using an unpaired t-test to compare length and width measures between sensitive and resistant strains. (A) Mean hemozoin length was 492.7nm ± 25.5nm for NF54, 470.1nm ± 29.7nm for 3D7, and 440.5nm ± 70.6nm for HB3. N=50, n=38, and n=5 individual crystals were measured for each respective CQS strain. Mean hemozoin length was 499.5nm ± 21.9nm for ITG, 461.6nm ± 16.7nm for DD2, and 464.2nm ± 22.6nm for FCR3. N=50, n=3, and n=5 individual crystals were measured for each respective CQR strain. No significant difference of crystal length was found between any CQS and CQR strains. (B) Mean hemozoin width was 114.1nm ± 4.9nm for NF54, 117.0nm ± 6.0nm for 3D7, and 122.9nm ± 13.3nm for HB3. N=25, n=45, and n=5 individual crystals were measured for each respective CQS strain. Mean hemozoin length was 115.2nm ± 5.8nm for ITG, 100.8nm ± 9.7nm for DD2, and 105.8nm ± 4.6nm for FCR3. N=25, n=5, and n=30 individual crystals were measured for each respective CQR strain. No significant difference of crystal width was found between any CQS and CQR strains.

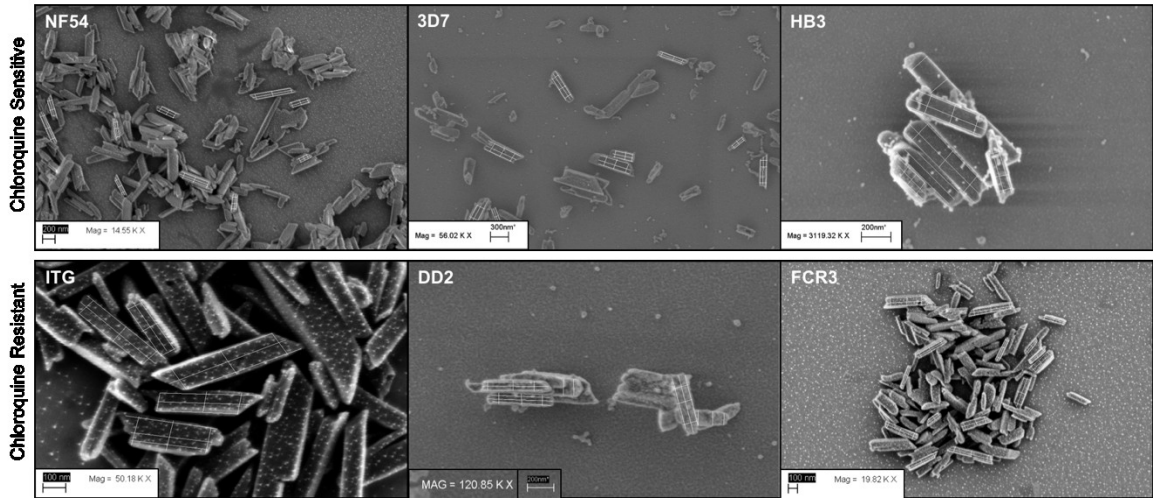

Fig. 2.7 Analyzed FEISEM images of non-isogenic *Pf* hemozoin.
Representative images of non-isogenic CQS and CQR *Pf* strains taken with FEISEM and analyzed using ImageJ. Markings used to measure crystal lengths and widths are visible in these images.

DISCUSSION

In this study we explored altered hemozoin production as a parasite stress response. This stems from the hypothesis that ring-stage artemisinin resistant parasites with shortened trophozoite stages exhibit altered hemozoin production. Because most hemozoin production occurs during the trophozoite stage, we predict that lesser time spent as a trophozoite would yield lesser amounts of hemozoin. However, it has been reported that ring-stage artemisinin resistant parasites with altered development produce the same amount of hemozoin as susceptible parasites with normal development [15]. Therefore, we explored the morphology of the hemozoin crystals being produced in order to learn more about the nucleation process of resistant parasites.

We began by measuring hemozoin dimensions from C580Y, a ring-stage artemisinin resistant strain, and found that hemozoin crystals were significantly smaller than the artemisinin susceptible CamWT. Additionally, we measured crystals from 106/1 and FCB, isogenic strains where a single point mutation K76T confers chloroquine resistance in FCB. In these isogenic strains we saw similar results in that the chloroquine resistant strain FCB produced smaller sized hemozoin crystals than 106/1. Therefore, we observed that a single point mutation which confers resistance may be sufficient to produce smaller sized hemozoin crystals as was seen in both C580Y and FCB as compared to their respective susceptible strains. Smaller sized hemozoin crystals were also observed in isogenic *P. berghei* resistant strains. However, hemozoin sizes were not significantly different when comparing non-isogenic chloroquine sensitive and resistant *P. falciparum* strains. Therefore, it may be that a single point mutation which confers resistance is necessary to produce smaller sized crystals. However, this needs to be

further explored in more drug susceptible and resistant isogenic strains to confirm that this is the case.

The implications of this research concern the mechanisms by which hemozoin is produced and how this is altered under drug pressure to confer resistance. The details underlying the process of hemozoin production remain to be clarified, however, there is increasing evidence of neutral lipid bodies in the digestive vacuole which promote hemozoin formation [16]. We hypothesize that hemozoin nucleation sites are producing smaller sized crystals as a result of a single point mutation which confers drug resistance. It has been reported that in C580Y, the same total amount of hemozoin is produced as CamWT [15]. In order to produce the same amount of total hemozoin while producing smaller sized crystals, we hypothesize an increase in the number of hemozoin nucleation sites within the digestive vacuole to compensate for hemozoin production during a shortened trophozoite stage. By increasing the number of hemozoin nucleation sites, parasites can potentially overcome pressure under drugs targeting hemoglobin degradation and hemozoin production by increasing their ability to continue these essential processes.

To further verify whether smaller sized hemozoin crystals are truly a product of single nucleotide polymorphisms in drug resistant parasites, we would like to measure hemozoin crystals of more drug susceptible and resistant isogenic *P. falciparum* strains. We would also like to confirm the total amounts of hemozoin being made by parasites with altered development. Finally, we would like to see whether drug pressure on susceptible strains alters hemozoin production. We attempted to do this by adding 1uM drug (chloroquine, artesunate, pyronaridine) to C580Y cultures for a 4 hour drug pulse at

trophozoites. However, we believe this dose may be too strong to potentially observe changes in hemozoin production. Applying drug at lower concentrations and during early ring into trophozoite stages may allow us to collect a measurable amount of hemozoin for morphology analysis. We predict that with constant drug pressure on sensitive strains, the parasites may develop the ability to produce smaller sized crystals. Measuring the total amount of hemozoin production along with the sizes of the crystals produced will provide further insight into how hemozoin is produced and how this process is altered as a parasite becomes drug resistant.

REFERENCES

1. Tilley L, Straimer J, Gnädig NF, Ralph SA, Fidock DA. Artemisinin action and resistance in *Plasmodium falciparum*. Trends Parasitol [Internet]. Elsevier Ltd; 2016;32:682–96. Available from: http://dx.doi.org/10.1016/j.pt.2016.05.010

2. Meshnick SR. Artemisinin: mechanisms of action, resistance and toxicity. Int J Parasitol. 2002;32:1655–60.

3. Blasco B, Leroy Di, Fidock DA. Antimalarial drug resistance: Linking *Plasmodium falciparum* parasite biology to the clinic. Nat Med. 2017;23:917–28.

4. Dondorp AM, Nosten F, Yi P, Das D, Phyo AP, Tarning J, et al. Artemisinin resistance in *Plasmodium falciparum* malaria. N Engl J Med. 2009;365:455–67.

5. Witkowski B, Amaratunga C, Khim N, Sreng S, Chim P, Kim S, et al. Novel phenotypic assays for the detection of artemisinin-resistant *Plasmodium falciparum* malaria in Cambodia: *in-vitro* and *ex-vivo* drug-response studies. Lancet Infect Dis. 2013;13:1043–9.

6. Ariey F, Witkowski B, Amaratunga C, Beghain J, Langlois AC, Khim N, et al. A molecular marker of artemisinin-resistant *Plasmodium falciparum* malaria. Nature. 2014;505:50–5.

7. Straimer J, Gnadig NF, Witkowski B, Amaratunga C, Duru V, Ramadani AP, et al. K13-Propeller mutations confer artemisinin resistance in *Plasmodium falciparum* clinical isolates. Science (80-). 2015;347:428–31.

8. Mok S, Ashley EA, Ferreira PE, Zhu L, Lin Z, Chotivanich K, et al. Population transcriptomics of human malaria parasites reveals the mechanism of artemisinin resistance. Science (80-). 2017;347:431–5.

9. Hott A, Casandra D, Sparks KN, Morton LC, Castanares GG, Rutter A, et al. Artemisinin-resistant *Plasmodium falciparum* parasites exhibit altered patterns of development in infected erythrocytes. Antimicrob Agents Chemother. 2015;59:3156–67.

10. Gorka AP, Alumasa JN, Sherlach KS, Jacobs LM, Nickley KB, Brower JP, et al. Cytostatic versus cytocidal activities of chloroquine analogues and inhibition of hemozoin crystal growth. Antimicrob Agents Chemother. 2013;57:356–64.

11. Noland GS, Briones N, Sullivan DJ. The shape and size of hemozoin crystals distinguishes diverse *Plasmodium* species. Mol Biochem Parasitol. 2003;130:91–9.

12. Cooper RA. Alternative mutations at position 76 of the vacuolar transmembrane protein PfCRT are associated with chloroquine resistance and unique stereospecific quinine and quinidine responses in *Plasmodium falciparum*. Mol Pharmacol. 2003;61:35–42.

13. Fitch CD, Yunis NG, Chevli R, Gonzalez Y. High-affinity accumulation of chloroquine by mouse erythrocytes infected with *Plasmodium berghei*. J Clin Invest. 1974;54:24–33.

14. Pisciotta JM, Scholl PF, Shuman JL, Shualev V, Sullivan DJ. Quantitative characterization of hemozoin in *Plasmodium berghei* and *vivax*. Int J Parasitol Drugs Drug Resist [Internet]. Elsevier Ltd; 2017;7:110–9. Available from: http://dx.doi.org/10.1016/j.ijpddr.2017.02.001

15. Heller LE, Roepe PD. Quantification of free ferriprotoporphyrin IX heme and hemozoin for artemisinin sensitive versus delayed clearance phenotype *Plasmodium falciparum* malarial parasites. Biochemistry. American Chemical Society; 2018;57:6927–34.

16. Pisciotta JM, Coppens I, Tripathi AK, Scholl PF, Shuman J, Shulaev V, et al. The role of neutral lipid nanospheres in *Plasmodium falciparum* haem crystallization. Biochem J. 2007;402:197–204.

CHAPTER 3

QUANTIFYING THE COMPARTMENTAL KINETICS OF HEMOZOIN DURING CLEARANCE OF INFECTION

INTRODUCTION

To improve on current diagnostics, hemozoin is a potential biomarker for malaria infections. However, the most popular methods of hemozoin detection have their limits if they were to be used as diagnostics. Where mass spectrometry and powerful microscopy are efficient ways of detecting hemozoin, they are not feasible to conduct in the field as malaria diagnostics. Exploiting the magneto-optical properties of hemozoin as a molecular biomarker is currently being explored [1]. To further establish hemozoin as a molecular biomarker of malaria, it is important to understand its kinetics during infection. Historically, autopsies of malaria patients have shown darkly pigmented organs such as the brain, liver, and spleen [2]. In blood, hemozoin can be ingested by monocytes and macrophages as these immune cells are phagocytosing infected and lysed RBCs. In tissue, resident macrophages may also be picking up hemozoin resulting in sequestered pigment within the organs[3]. It is hypothesized that hemozoin can have immunomodulatory effects on macrophages by suppressing their activity. Therefore, studying the kinetics of hemozoin in blood and tissue during infection can have important implications on further understanding the immune responses to *Plasmodium* infection.

Several studies have looked into hemozoin levels in blood and tissue of mouse models to quantify hemozoin during the course of an infection. One study used a fluorometric assay converting hemozoin to protoporphryn IX to measure its fluorescence [4]. In this study, mice were infected with two rodent malaria strains: *P. berghei* NK65 and *P. berghei* ANKA. They collected whole blood, livers, and spleens at different time points in the *Pb*NK65 infected mice. These mice were followed out until day 18 post infection. The *Pb*ANKA model was used to look at hemozoin in cerebral malaria. This

study showed that over the course of 18 days, hemozoin concentration in the livers and spleens of infected mice increased exponentially, and that this correlated with the duration of infection [4]. It seemed that hemozoin accumulated more rapidly in the spleen, but greater overall accumulation occurred in the liver at day 18.

Another study looked at long term levels of hemozoin in the livers and spleens of mice infected with *P. yoelii and P. chabaudi* after infection had cleared [5]. In *P. yoelii* infected mice there was no change in liver concentration of hemozoin, however there was a 5-fold increase in spleen concentration at day 270 post parasite clearance. In the *P. chabaudi* infected mice, there was a 70% decrease in liver concentration and a 3-fold increase in spleen concentration at day 270 as well. A decrease in liver concentration and increase in spleen concentration suggests that hemozoin may translocate from the liver to the spleen. This study also showed that hemozoin can persist in the tissues up to 9 months after clearance of infection [5]. Another study of the long term kinetics of hemozoin presented similar findings in that hemozoin levels decreased in the liver and increased in the spleen but was present up to 196 days after chloroquine treatment [6].

The transport of hemozoin from the liver to the spleen during clearance of infection presumably occurs via the blood. Hemozoin in whole blood can be quantified by spectrophotometry. However, in one of the studies quantifying hemozoin in blood, no hemozoin was quantified in up to 320ul of plasma [7]. It is possible that hemozoin may exist in plasma as residual parasite proteins and hemozoin are left in a once-infected RBC after rupture. Therefore, spectrophotometry may not have been a sensitive enough method to quantify hemozoin in plasma. In exploring more sensitive assays to quantify hemozoin, luminescence based assays seem promising. Luminol is a substance that can

react with heme iron and exhibit chemiluminescence under the appropriate conditions. Interestingly, luminol is commonly used by forensic scientists to detect trace amounts of blood. The reaction between luminol and heme iron can be exploited to create a more sensitive quantitative assay for hemozoin. Deroost et al. were able to show that a heme-enhanced luminescence based system could quantify hematin down to concentrations of 100 nM as compared to 1 uM concentrations quantified using absorbance [8].

The goal of this project was to use the heme-enhanced luminescence based system to develop a sensitive assay for hemozoin quantification in human and mouse whole blood fractions. By developing a more sensitive quantitative assay, we aim to compare hemozoin concentrations between the RBC and plasma fractions of whole blood. We hypothesize that during initial clearance of infection, hemozoin will be more concentrated in the RBC fraction. However, after clearance through the spleen, residual hemozoin may be present in the plasma. This project will allow for us to better understand the compartmental kinetics of hemozoin during clearance of infection, with larger implications of understanding the general kinetics of hemozoin to develop diagnostics and elucidate immunomodulatory mechanisms.

METHODS

Ethics approval

De-identified human patient whole blood samples were collected under the approved Johns Hopkins School of Public Health IRB protocol #9164. Animal experiments were performed under the approved protocol MO16H91.

Patient blood collection

Plasmodium infected human patient whole blood samples were collected from the Johns Hopkins Hospital Microbiology Lab and de-identified. 50 ul whole blood was aliquoted and the rest of the sample was centrifuged at 7600 rpm for 4.5 mins to separate into RBC and plasma fractions. The RBC fraction was washed with PBS a total of 4 times. All samples were stored in -80°C until processing.

Although the patient samples were de-identified, information such as *Plasmodium* species of infection, date and time of blood draw, treatment, days post treatment, and parasitemia were included upon collection.

Mouse tissue and blood collection

Mice treated with a curative dose of pyronaridine were sacrificed at 0, 1, 2, 4, 7, 10, 13, 25, 86, and 100 days post treatment to harvest their livers, spleens, and whole blood for hemozoin quantification. Tissue masses were recorded upon harvest. 100ul whole blood was aliquoted for hemozoin purification and the rest was fractionated into RBC and plasma aliquots as previously described. In contrast to the human samples, the RBC fraction was not washed with PBS to preserve any white blood cells (WBCs). All samples were stored at -80°C until processing.

A total of 127 mice were used for this study. The mice were classified into different groups based on initial parasitemia and development of infection. Single peak parasitemia occurred in mice that were treated when a single curative dose of pyronaridine was given at peak parasitemia. Double peak parasitemia occurred in mice that were drug treated at the first peak of parasitemia, followed by a decline in parasite burden, after which infection recurred to a second peak at which time they were treated with a curative dose of pyronaridine. A summary of the mouse harvests can be found in Table 3.1.

Table 3.1 Mouse experiment summary.
The number of processed samples for liver, spleen, whole blood, RBC, and plasma per day post treatment in *P. berghei* infected white mice are presented.

			Tissue samples processed		Blood samples processed		
Day post treatment	Total # of mice	Parasitemia peak	Liver	Spleen	WB	RBC	Plasma
0	24	1,2	5	20	17	17	17
1	5	2	3	5	5	5	5
2	19	2	3	9	19	19	19
4	5	2	3	5	5	5	5
7	15	2	5	15	15	15	15
10	14	2	3	14	14	14	14
13	5	2	3	5	5	5	5
25	13	1	3	13	13	13	13
86	10	2	3	10	10	10	10
100	17	1	3	17	17	17	17

Hemozoin purification

All samples were thawed and processed to purify and quantify hemozoin. The protocol with which hemozoin was purified from blood and tissue was adapted from Pisciotta et al. [7] Mouse livers and spleens were homogenized in 5 ml and 1 ml of water respectively using pulse sonication (Branson Sonifier 250). They were then centrifuged at 13000 rpm for 10 mins after which the supernatant was discarded. 1 ml 2%SDS/100mM sodium bicarbonate (pH 9.2) was added to each sample and sonicated. Samples were centrifuged at 13000 rpm for 5 mins. The supernatant was discarded along with any

solubilized free heme within it. 1 ml proteinase K dissolved in protease K buffer (10 mM Tris pH 8, 0.5% SDS, 1 mM CaCl2) at 1 mg/ml was added to each sample and sonicated. The samples were left to incubate in a 60°C water bath overnight. After incubation, samples were centrifuged at 13000 rpm for 5 mins and the supernatant was discarded. Another 1ml of 2%SDS/100mM sodium bicarbonate was added to each sample and sonicated. After centrifugation the supernatant was removed. At least two more wash steps were performed with 1ml 2% SDS until the supernatant was clear after centrifugation. After the final wash, purified hemozoin from livers and spleens were resuspended in 1 ml and 500 ul of 2% SDS respectively and sonicated.

All whole blood, red blood cell (RBC), and plasma samples were purified using a similar but modified version of the previously described protocol. The samples were lysed with water by bringing each sample up to 1 ml. An additional 10 ul of 10% SDS was added to each mouse sample. Samples were vortexed and centrifuged at 13000 rpm for 5mins and the supernatant was discarded. 2x 2%SDS/100mM sodium bicarbonate washes and 2x 2% SDS washes were performed as previously described. After the final wash, samples were resuspended in 250ul 2%SDS/50mM NaOH and vortexed. With each processing batch of whole blood, RBC, and plasma samples, at least two positive and two negative controls were processed as well. For the whole blood negative controls, 200ul of uninfected human RBCs at 50% hematocrit in PBS was processed. For the RBC negative controls, 100 ul of uninfected human packed RBCs was processed. For the plasma controls, 100 ul of uninfected human serum was processed. Positive controls were created by adding 10 nmol of β-hematin to each negative control condition.

Hemozoin quantification using absorbance

Highly concentrated samples with a visible black hemozoin pellet after purification were quantified using visible spectrophotometry at 405nm. 10-50 ul of each sample were plated in duplicate in a 96-well clear flat-bottom plate. Each well was brought up to a volume of 200 ul with 2%SDS/50 mM NaOH to de-crystallize the hemozoin. A hemin standard curve was developed and plated in duplicate within a concentration range of 0.8 – 10 nmol/well. 100 ul of 2% SDS was also plated in duplicate to measure background noise. Both the hemin standards and 2% SDS wells were also brought up to 200 ul in 2%SDS/50 mM NaOH. The plate was left to incubate at room temperature for 30 mins before being read on the SpectraMax M2 plate reader. Hemozoin concentration of samples with an optical density within the limits of quantification was determined by developing a linear regression of the hemin standard curve. The linear regression equation was used to calculate the hemozoin concentration of each well from the mean optical density of each pair of duplicate wells. Samples which were too highly saturated were diluted down to the quantifiable range of measuring hemozoin with absorbance.

Hemozoin quantification using luminescence

Samples in which there was no visible hemozoin were quantified with a luminol assay we optimized from [8]. After having been already de-crystallized in 2%SDS/50 mM NaOH, a maximum of 200 ul of each sample was plated in a 96-well black flat-bottom plate. A hemin standard curve was also developed for this assay and was plated in duplicate at ranges from 0.8-10 pmol/well. Additionally, 100 ul 2% SDS was plated in duplicate to measure background noise. Wells containing the hemin standard curve and

2% SDS were brought up to 200 ul in 2%SDS/ 50 mM NaOH. 75 ul of luminol at 100ug/ml in luminol reagent (4 volumes of 100 mM NaOH, 2% SDS, 3 mM EDTA to 1 volume of 1M Na_2CO_3) was added to each well [8]. Immediately before reading the plate, 25 ul of 7% H_2O_2 (diluted from a 31% stock in the same 4:1 luminol reagent) was added to each well. Peroxide is catalyzed into oxygen by Fe^{3+}, which reacts with the luminol to produce luminescence. We captured the luminescence emitted from each well with a 1s exposure on the IVIS Spectrum imager. The software program Living Image was used to quantify luminescence in photons/sec for each well. Similar to the absorbance assay, we used a linear regression equation from the hemin standard curve to quantify the amount of hemozoin in each well from which we were able to determine the hemozoin concentration of the original sample.

Data analysis

Samples were quantified against a hemin standard curve developed for each appropriate assay. For all blood samples processed, average background luminescence from the negative controls processed with that batch of samples was subtracted from individual luminescence of each infected sample before calculating hemozoin concentration. All data was plotted and analyzed using GraphPad Prism 6.

RESULTS

Luminol assay is a more sensitive method of hemozoin quantification than absorbance.

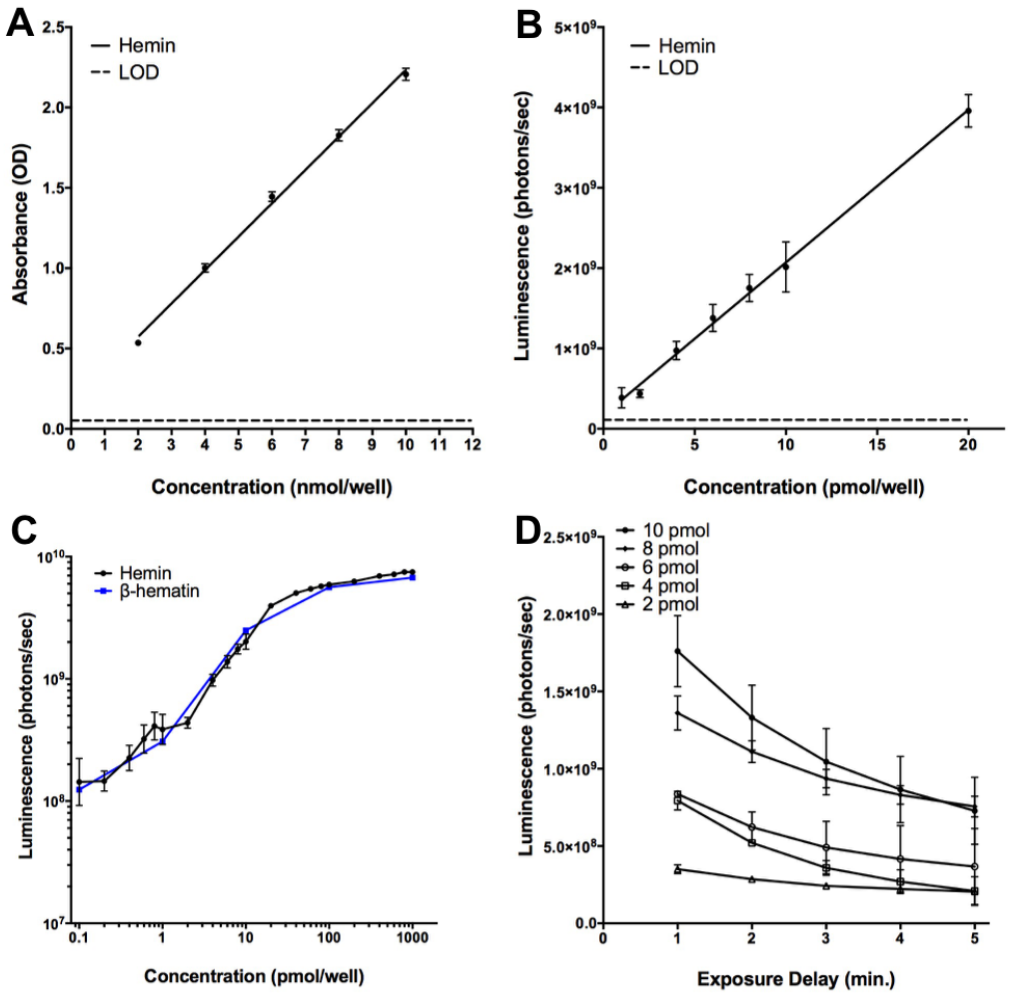

Fig. 3.1 Hemin standard curves.
Standard curves were developed with hemin for hemozoin quantification assays. (A) Hemin standard curve for quantification using absorbance. Mean OD values for 10 biological replicates were plotted with error bars depicting SEM. R^2 for this linear regression model (solid line) was 0.97. Average LOD for replicate runs was 0.052 (dashed line). (B) Hemin standard curve for quantification using luminescence. Mean luminescence in photons/sec for 11 biological replicates were plotted with error bars depicting SEM. R^2 for this linear regression model (solid line) was 0.80. Average LOD for replicate runs was 8.250e7 (dashed line). (C) Hemin standard curve on luminol assay is representative to luminescence from β-hematin at equivalent concentrations. (D) Time course of hemin luminescence. 1 sec. exposure with 1 sec. delay of hemin was analyzed over the course of 5 mins.

Two methods of hemozoin quantification were utilized for this project. First, hemozoin was quantified by measuring its optical density after de-crystallization. A standard curve for this assay was developed using hemin. Background from 100 ul 2% SDS was measured in duplicate on each plate and averaged over 10 plates to get an optical density of 0.046. The LOD of each plate was determined by adding three standard deviations to the mean background value resulting in a mean LOD of 0.052, as depicted as the dashed line in Fig. 3.1A. By plating a range of hemin concentrations, the lower limit of quantification was determined to be 600 pmol hemin in 200 ul per well with an OD of around 0.2. Any samples with an OD of under 0.2 were considered to be too low in concentration to be quantifiable by absorbance. Saturation occurred at an OD of 2.5, therefore samples with an OD above this value were diluted down to be re-quantified. A hemin standard curve with concentrations ranging from 2 nmol to 10 nmol on each plate analysis was used to create a linear regression model with which unknown samples could be quantified.

A similar method was used to develop a hemin standard curve for the luminol assay. The lower limit of quantification by luminol was determined to be at a hemin concentration of 400 fmol in 200 ul per well with a luminescence of around 2.25e8 photons/sec. Saturation in the luminol assay occurred at around 4e9 photons/sec. The mean limit of detection over 11 replicates of standard curves was 8.250e7 as depicted with the dashed line in Fig. 3.1B. By developing this standard curve we were able to establish that the luminol assay is a one thousand-fold more sensitive method of quantification of heme with an LOQ of 400 fmol as compared to absorbance which has

an LOQ of 600 pmol. This one thousand-fold increase in sensitivity allowed us to quantify heme samples that were too low to have a detectable optical density.

Luminescence of hemin was compared to that of β-hematin to ensure the hemin standard curve would accurately represent hemozoin concentrations. Known equivalent amounts of hemin and β-hematin were analyzed on the luminol assay. As shown in Fig. 3.1C, luminescence values for both hemin and β-hematin overlap nicely at equivalent concentrations within quantifiable range.

A time course was performed with a 1 second exposure and 1 minute delay over 5 minutes with a range of hemin concentrations. As presented in Fig. 3.1D, luminescence peaks at the first exposure and then gradually declines.

Hemozoin is transported from the liver to spleen via whole blood during clearance of infection.

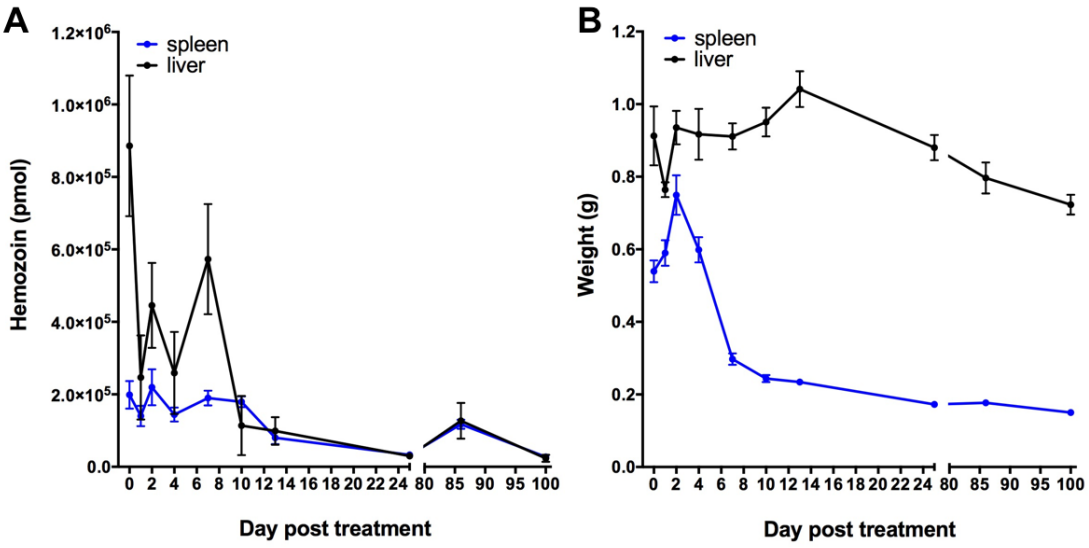

Fig. 3.2 Total hemozoin content in mouse livers and spleen.
(A) Mean values of total hemozoin (in pmol) purified from tissue is plotted per day post pyronaridine treatment. Error bars indicate SEM. (B) Mean values of tissue weights taken at time of harvest is plotted with error bars indicating SEM. N of samples at each day can be found in Table 3.2.

Hemozoin was isolated from livers and spleens of mice after 0, 1, 2, 4, 7, 10, 13, 25, 86, and 100 days post treatment with a curative dose of pyronaridine. Hemozoin isolated from livers and spleens was quantified using absorbance. Figure 3.2A presents total hemozoin content isolated from the full livers and spleens. The weight of each individual organ was recorded at the time of harvest (Fig 3.2B). Livers weighed between 800 mg – 1g during the first two weeks post treatment after which the sizes grew smaller. Spleens weighed around 600 mg during the first 4 days post treatment with the exception of day 2 spleens which were similar in weight to the livers at day 2. After day 4, spleen weight declined as well. There appears to be more total hemozoin in the liver up to day 10 post treatment after which the total amount of hemozoin is the same in the liver and the spleen.

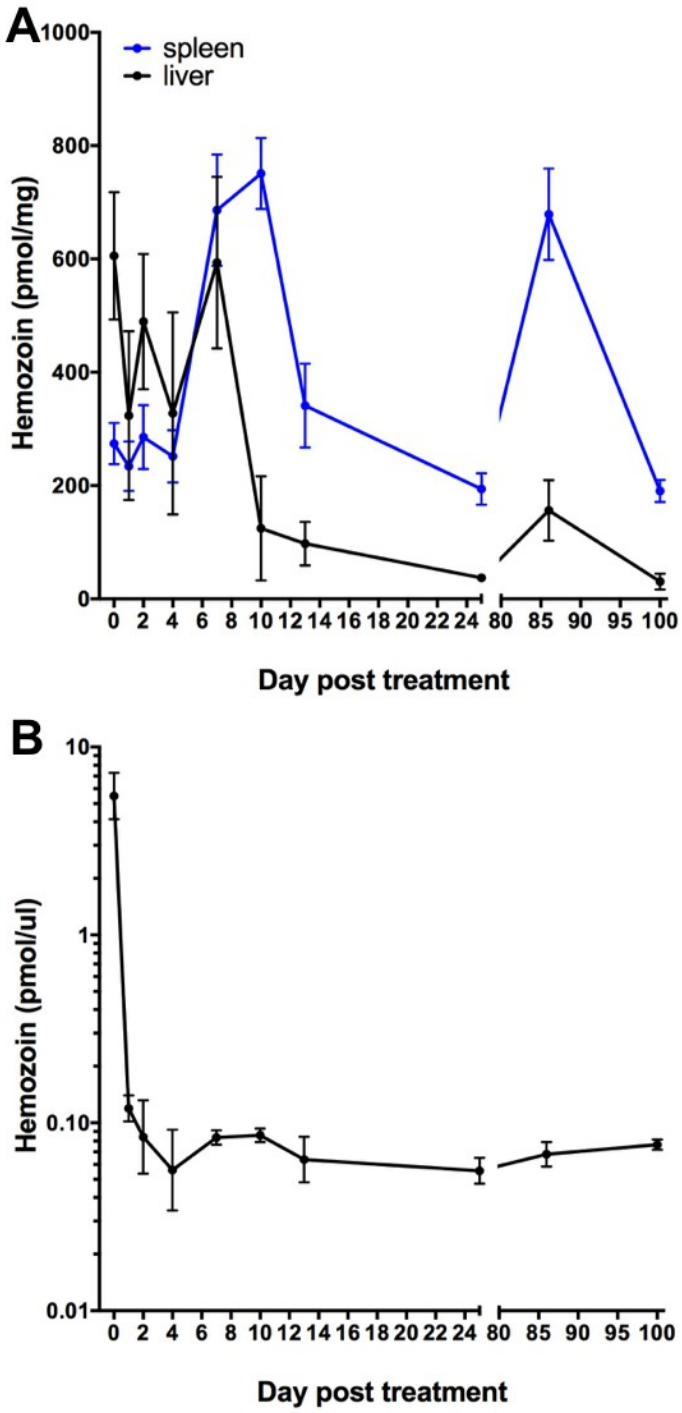

Fig. 3.3 Hemozoin concentration in mouse livers, spleens, and whole blood.
(A) Isolated hemozoin from mouse livers and spleens was quantified using absorbance. Mean values of pmol hemozoin per mg tissue processed from individual mice are plotted for each day post treatment. Error bars represent SEM. (B) Isolated hemozoin from 100 ul whole blood (WB) was quantified using luminescence. Mean values of pmol hemozoin per ul WB processed are plotted for each day post treatment. Error bars represent SEM.

Table 3.2 Mean ± SEM hemozoin concentration in liver, spleen and WB.
Liver and spleen samples were quantified using absorbance and are presented in pmol hemozoin per mg tissue processed. WB samples were quantified using luminescence and are presented as pmol hemozoin per ul WB processed.

	Liver		Spleen		WB	
Day post treatment	N	Mean ± SEM (pmol/mg)	N	Mean ± SEM (pmol/mg)	N	Mean ± SEM (pmol/ul)
0	5	605 ± 112	20	274 ± 35	6	5.492 ± 1.795
1	3	323 ± 149	5	234 ± 44	4	0.119 ± 0.020
2	3	490 ± 119	9	286 ± 57	10	0.084 ± 0.048
4	3	328 ± 178	5	251 ± 46	2	0.056 ± 0.036
7	5	594 ± 151	15	686 ± 99	15	0.083 ± 0.008
10	3	124 ± 92	14	750 ± 63	14	0.086 ± 0.007
13	3	98 ± 39	5	341 ± 74	5	0.064 ± 0.020
25	3	37 ± 8	13	194 ± 28	9	0.056 ± 0.009
86	3	156 ± 53	10	679 ± 81	9	0.068 ± 0.011
100	3	31 ± 14	17	190 ± 20	17	0.076 ± 0.005

Fig. 3.3A presents the hemozoin concentration normalized to tissue weight. There is a significantly larger amount of hemozoin concentrated in the liver during the first four days of clearance post treatment. After day 7, hemozoin concentrations in the spleen increase to larger amounts than the liver. Concentrations in the liver peak at day 10 and then decline. An additional peak in both liver and spleen concentrations is observed at day 86, followed by a decline to day 100.

Hemozoin from 100ul whole blood was also isolated for each mouse. Fig. 3.3B presents quantification of hemozoin by luminescence from these samples by plotting the mean values from individual mice over the course of clearance. Hemozoin levels were extremely high on day 0 relative to the rest of the days. Hemozoin concentration in whole blood rapidly declines on day 1 and continues to do so until day 4. This is followed by an increase and subsequent peak in hemozoin concentration between days 4 and 10 after which hemozoin levels decline again and remain constant out through day 100. Hemozoin concentrations presented in Fig. 3.3B were calculated after subtracting out background luminescence. The number of samples which remained positive above the

background threshold and the mean hemozoin concentrations of these samples can be found in Table 3.2.

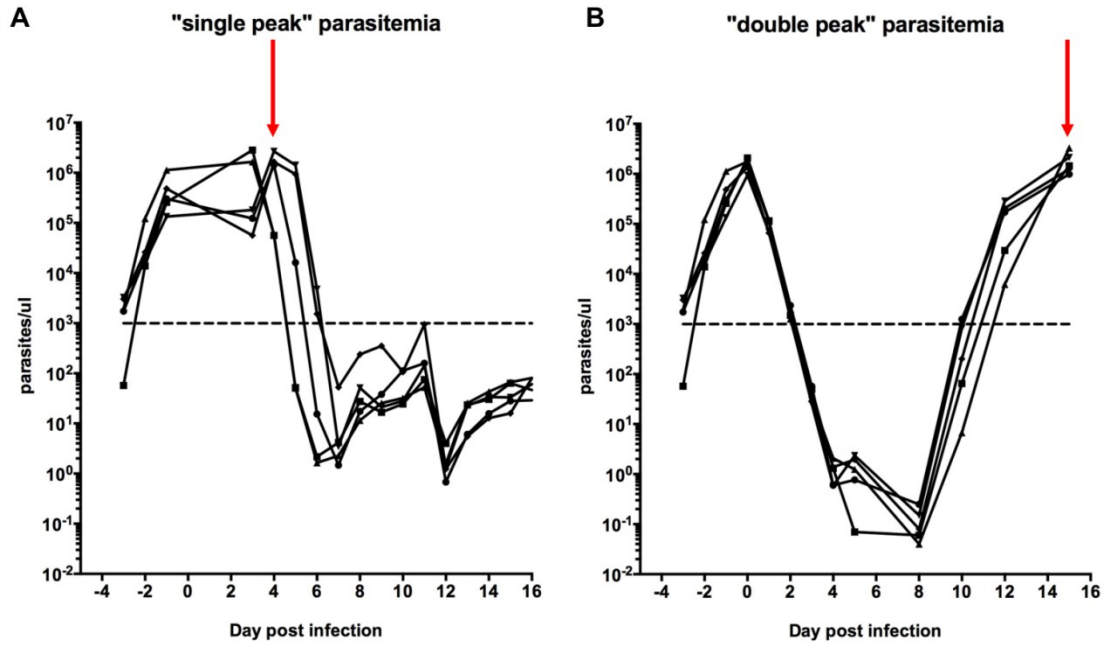

Fig. 3.4 Single and double peak parasitemia in *P. berghei* infected mice.
Mice were classified into two groups of parasitemia. Parasitemia was determined by luciferase and is presented in parasites/ul of blood. Baseline detection of the luciferase assay is plotted as the dashed line (---) at 1000 parasites/ul. This figure presents 5 representative mice from each group. The red arrow indicates when pyronaridine was given. (A) Single peak mice received pyronaridine at peak parasitemia after which parasite concentration decreased (B) Double peak mice received pyronaridine at the second peak of parasitemia after recurrence of infection.

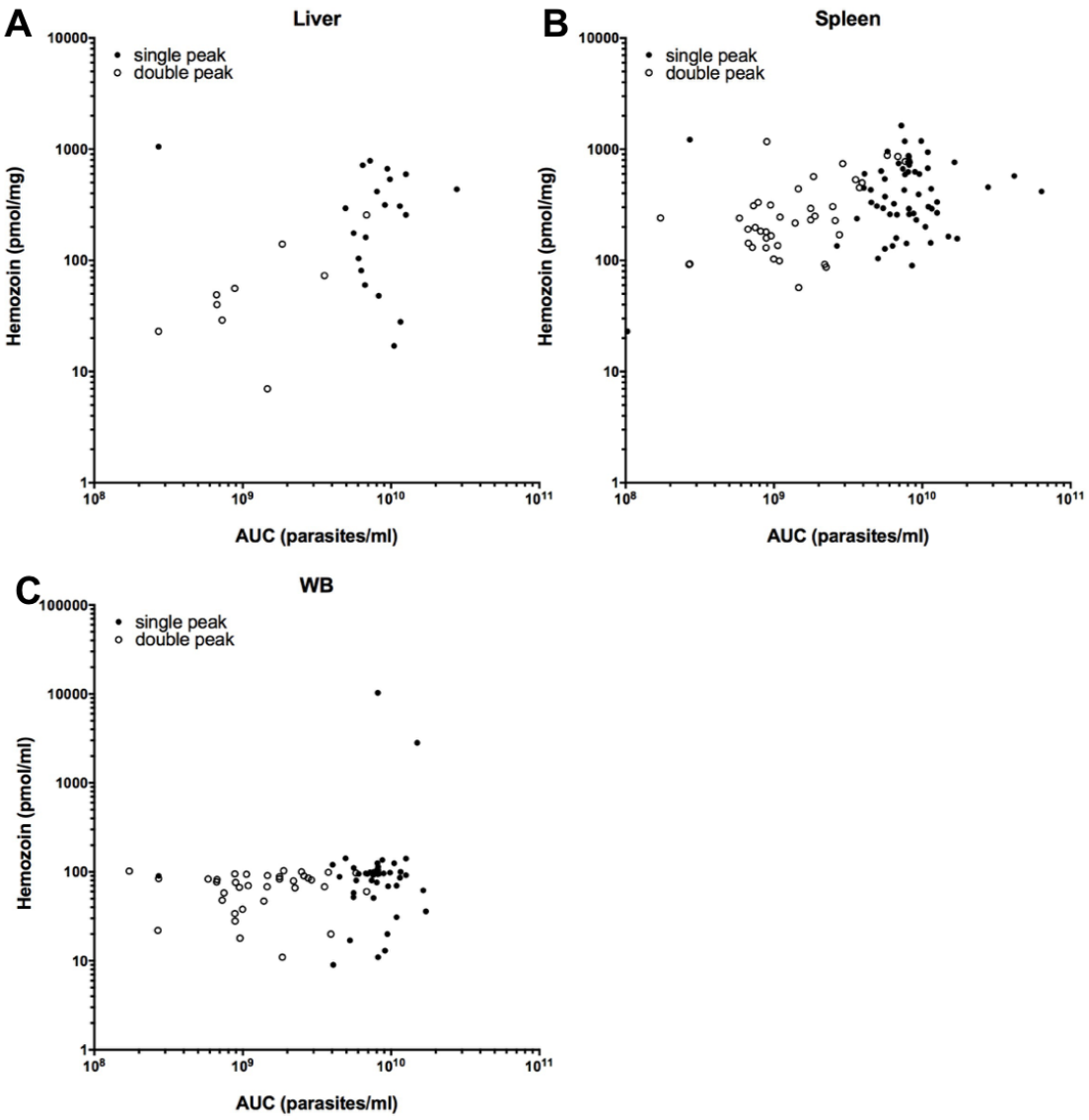

Fig. 3.5 Parasitemia of individual mice compared to hemozoin concentration in liver, spleen, and whole blood.
Parasite burden for each mouse was calculated by determining the area under the parasitemia curve before pyronaridine treatment. AUC was converted to parasites/ml of blood. Parasitemia in mice was determined using a luciferase assay. (A) Parasite burden of all individual mice is plotted against matched liver concentrations. (B) Parasite burden of all individual mice is plotted against matched spleen concentrations. (C) Parasite burden of all individual mice is plotted against matched WB concentrations.

We wanted to determine whether total parasite burden correlated with the amount of hemozoin present in mouse tissue and whole blood. Mice were classified into single and double peak parasitemias of which the area under the curve (AUC) was calculated in

parasites/ul. Single peak mice received pyronaridine at peak parasitemia after which parasite concentration decreased (Fig. 3.4A). The average area under the curve for all single peak mice was roughly 2 million parasites/ul. Single peak mice were harvested at days 0, 25, and 100 post drug treatment. Double peak mice received pyronaridine at the second peak of parasitemia after recurrence of infection (Fig. 3.4B). The average area under the curve for all double peak mice was roughly 9 million parasites/ul. Double peak mice were harvested at days 0, 1, 2, 4, 7, 10, 13, and 86 post drug treatment. Naturally, single peak mice had an overall lower parasite burden than double peak mice due to recurrence of infection in the double peak mice. There is no general trend between parasite burden and hemozoin concentration in the livers, spleens, and whole blood (Fig 3.5). This relationship was also analyzed by each day and no significant trend was found. High hemozoin concentration in whole blood may be attributed to a higher parasite burden; however, this is only seen in two samples (Fig. 3.5C).

Hemozoin is quantifiable in RBC and plasma fractions of whole blood in mice.

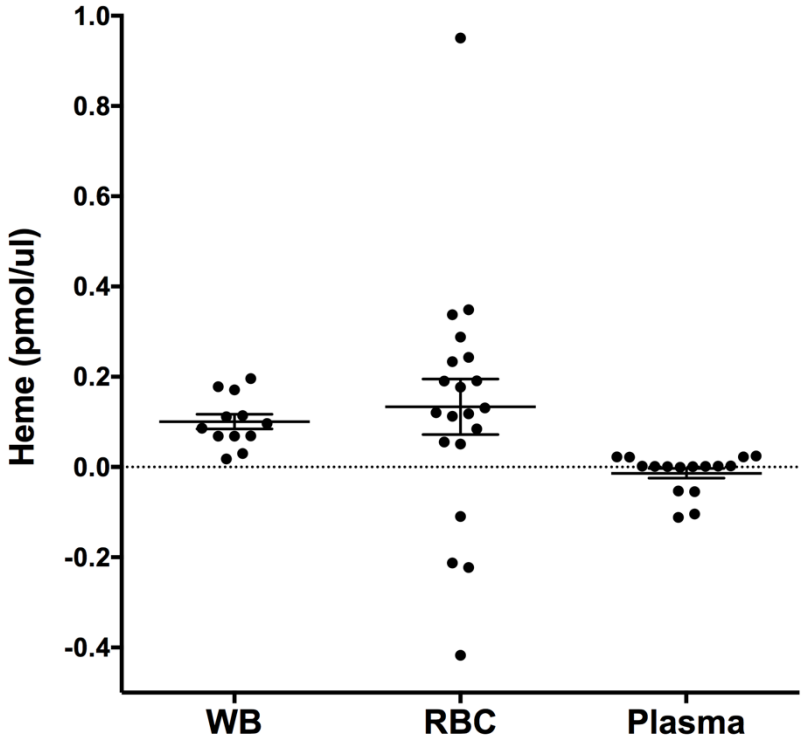

Fig. 3.6 Heme concentration in negative controls.
Negative controls purified alongside samples were quantified using luminol to assess background heme levels. Average heme concentrations were 0.101 ± 0.016 pmol/ul, 0.112 ± 0.076 pmol/ul, and <0 pmol/ul in WB, RBC, and plasma negative controls respectively. Negative or zero values represent no heme detection in that sample.

To ensure quantification of hemozoin heme and not free heme from the blood samples, we developed and processed representative negative controls alongside each batch of samples. Fig. 3.6 shows the calculated heme concentrations of individual negative controls processed with whole blood, RBC, and plasma samples and quantified using luminol. The plasma negative controls showed no quantifiable heme after purification. WB negative controls had 0.1 ± 0.016 pmol/ul heme after purification. Packed RBC negative controls had 0.1 ± 0.076 pmol/ul heme. Although the mean concentrations of heme between WB and packed RBCs is the same, we saw a larger deviation between biological replicates of RBC negative controls. As a result, a higher

background luminescence was subtracted from RBC samples before calculating their hemozoin concentration.

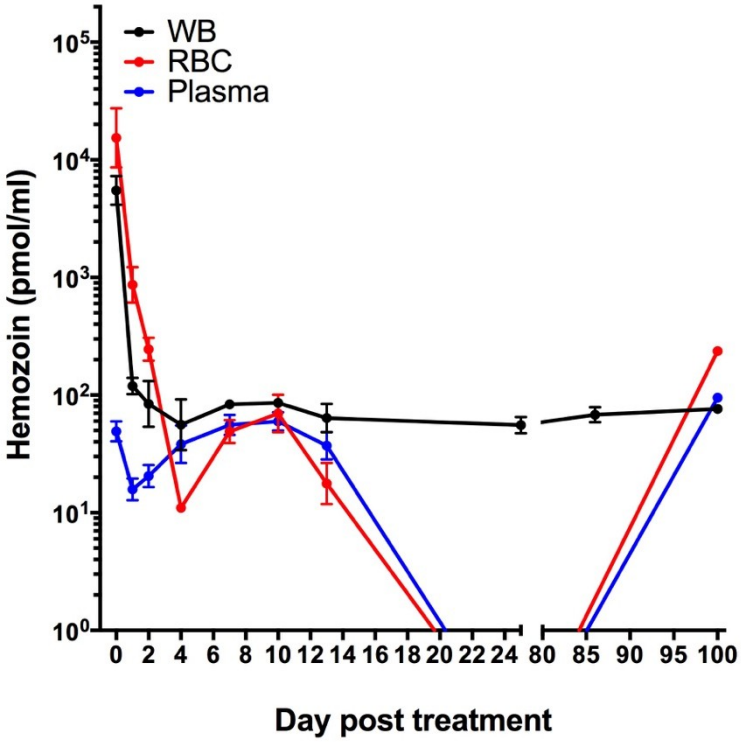

Fig. 3.7 Hemozoin quantified in WB, RBC, and plasma fractions in mice.
Mean values of hemozoin concentration in WB as well as RBC and plasma fractions are plotted over clearance of infection in days post treatment. Individual concentrations were calculated by subtracting out background luminescence from the average negative control. N of samples positively quantified on each day can be found in Table 3.3. Error bars depict SEM.

Of the 120 whole blood samples processed, 91 samples were quantifiable above negative control background for hemozoin using the luminol assay. Positive quantifiable samples were determined by subtracting out average background luminescence of the negative controls from each sample. Only 39 RBC samples were positive for hemozoin whereas 60 samples were positive in the plasma. Table 3.3 presents a distribution of the positive and negative RBC and plasma samples by each day. As mentioned previously, negative controls for RBC samples had a higher concentration of residual heme after

purification. However, samples with lower concentrations of heme are not attributed to higher negative control values. All plasma samples were quantifiable up until day 4 whereas a fewer number of RBC samples were positive for those same days. At day 7 and later, a similar number of samples were quantifiable for each fraction.

Table 3.3 Distribution of positive and negative samples among all mouse RBC and plasma samples quantified.
Samples positive for hemozoin were able to be quantified above the negative control background. Samples below this threshold were considered negative for hemozoin or unquantifiable. Depicted in this table is the distribution of the number of individual positive and negative samples among RBC and plasma fractions in which hemozoin was quantified.

	RBC		Plasma	
Days post treatment	+	-	+	-
0	6	1	7	0
1	5	0	5	0
2	7	12	19	0
4	1	3	4	0
7	6	9	11	4
10	9	5	9	5
13	4	1	5	0
25	0	13	0	13
86	0	10	0	10
100	1	16	1	16

Fig. 3.7 presents mean hemozoin concentrations in WB, RBC, and plasma samples for each day post treatment. At days 0, 1, and 2 post treatment, there is a significantly higher amount of hemozoin in the RBC fraction as compared to plasma. Only 1 RBC sample was positive at day 4, therefore we do not know the significance of this concentration. Between days 4 and 10, there is an increase in both RBC and plasma concentrations, which is also reflected in the whole blood. At day 13, we see more hemozoin in the plasma than the RBC fraction. At day 100, hemozoin concentration increases to above plasma concentrations. However, there is only 1 sample that was positive for hemozoin in the RBC and plasma fractions at day 100, and no positive

samples at days 25 and 86, so the significance of these concentrations is unknown.

Hemozoin concentrations for matched RBC and plasma samples can be found in Table 3.4.

Table 3.4 Hemozoin concentration in RBC and plasma of matched positive mouse samples.
Positive samples were able to be quantified above negative control background. Matched samples are presented here along with the calculated hemozoin concentration for that fraction.

Day post treatment	RBC (pmol/ml)	Plasma (pmol/ml)
0	14156	63
0	74264	28
0	523	15
0	2199	33
0	427	79
0	680	36
1	804	15
1	308	5
1	2247	26
1	292	11
1	682	22
2	89	31
2	438	4
2	75	5
2	210	5
2	356	8
2	438	64
2	113	11
4	11	72
7	21	88
7	82	16
7	64	45
7	81	0.46
7	26	101
10	2	60
10	8	78
10	9	2
10	130	78
10	25	67
10	13	85
13	12	47
13	3	25
13	13	44
13	43	1
100	237	95

Hemozoin is quantifiable in RBC and plasma fractions of infected human whole blood.

Table 3.5 Hemozoin concentration in RBC and plasma fraction of infected human patient whole blood.
Patient RBC and plasma samples positively quantified for hemozoin are presented in pmol/ml. Information on days post treatment when the whole blood sample was collected and parasitemia by qPCR was only available for the *P. falciparum* infections.

Species	Patient	Days post treatment	qPCR (Par/µL)	RBC (pmol/ml)	Plasma (pmol/ml)	RBC:Plasma
P.falciparum	C	6	0	63	4	18
				153	5	30
P.vivax/ovale	H			612	29	21
P.falciparum	I	0.17	49,598	183	4	44
				623	6	100
				450	5	98
P.malariae	M			177	7	26
P.falciparum	O	0	50,398	37	4	9
		1	28,956	118	3	46
P.falciparum	Q	1.18	342,878	105	3	34
		0		8	5	2
		1		3	7	0
P.falciparum	T	2		6	1	5
P.falciparum	X			127	0	327
		0.04	325,415	427	25	17
P.falciparum	Y	0.06	336,967	115	5	25
P.falciparum	Z	1	2,112	278	2	179

We purified and quantified hemozoin in the RBC and plasma fractions of 18 human patient whole blood samples collected at different time points post treatment (days0-6) for a total of 45 paired samples. Of the 45 paired samples, hemozoin was quantifiable in both fractions of 17 samples among 10 patients. 19 samples were positive in the RBC fraction and 33 samples were positive in the plasma fraction. Negative RBC and plasma samples varied from patient to patient and did not correlate with days post treatment or parasitemia. Quantifiable hemozoin concentrations in RBC and plasma fractions of infected patient whole blood can be found in Table 3.5. Day post treatment

and parasitemia by qPCR data were only available for the *P. falciparum* infections. In the positive samples, hemozoin is consistently more concentrated in the RBC fraction as compared to plasma in all but 1 pair of samples. However, more plasma samples were able to be positively quantified over the negative controls as compared to the RBC samples. There are no consistent trends in the magnitude of difference between RBC and plasma concentrations.

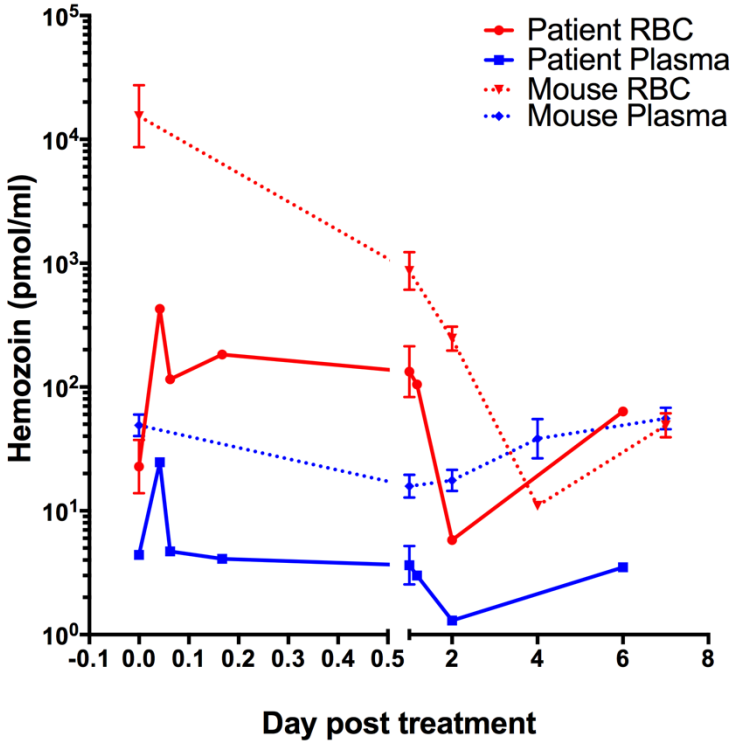

Fig. 3.8 Hemozoin concentrations in patients and mice over first week of clearance. Mean hemozoin concentration in RBC and plasma fractions of *P. falciparum* infected patients are plotted as the solid red and blue lines, respectively. Mean hemozoin concentration in RBC and plasma of *P. berghei* infected mice over the same range of days post treatment are plotted as the dashed red and blue lines, respectively. Error bars depict SEM.

RBC and plasma concentrations over the first week of clearance in patients and mice are compared in Fig. 3.8. Between days 0 and 2, RBC concentrations of hemozoin are consistently higher than plasma in both patients and mice. In patients, RBC

concentrations remain higher out to day 6 post treatment. However, for the patient data, we only have 1 pair of samples in which hemozoin was quantifiable for most time points. Time points with error bars (SEM) have a maximum N of 3 samples. The ratio between RBC and plasma concentrations also changes over time for both the mice and patients.

DISCUSSION

In order to explore the compartmental kinetics of hemozoin during clearance of infection we sought to develop a sensitive luminescence assay to quantify very small amounts of hemozoin. By de-crystallizing hemozoin in NaOH, we can exploit the inherent reaction between heme and H_2O_2 combined with luminol to detect fmol to pmol amounts of heme. We demonstrated this by developing a standard curve on the luminol assay using hemin in which our lower limit of quantification was 400 fmol heme in a volume of 200 ul. This was a 1000-fold increase in sensitivity as compared to measuring absorbance at 405 nm on a spectrophotometer. In an equivalent volume on the spectrophotometer, the limit of quantification was 600 pmol. The 96-well plate format of the luminol assay allows for sensitive quantification of hemozoin in volumes less than 200ul in a high-throughput format. With a strong imaging system, luminescence from each well can be precisely captured and converted to the number of photons emitted per second. Because the luminol reaction occurs rapidly after the addition of H_2O_2, it is necessary to minimize the amount of time between this step and imaging. However, a time course analysis shows that luminescence degrades over time; therefore, a 1 second exposure captures the peak of the reaction. With this fast, high-throughput luminol assay, we were able to quantify purified hemozoin from blood samples which were undetectable by optical density.

We used *P. berghei* infected white mice to model clearance of infection after a curative dose of pyronaridine at peak parasitemia. At days 0, 1, 2, 4, 7, 10, 13, 25, 86, and 100 post treatment, we harvested whole blood, livers, and spleens to purify and quantify hemozoin. In previous studies, hemozoin concentration in mouse livers and spleens

rapidly increased during infection [4]. In a long term study analyzing hemozoin during clearance of infection, hemozoin appeared to move from the liver to the spleen [5]. We observed a rapid decline in liver concentration (normalized to tissue weight) along with a rapid increase in spleen concentration (also normalized) between days 4 and 7 post treatment. Where during the first week of clearance, hemozoin concentration is significantly higher in the liver, after day 7, it is significantly higher in the spleen. When looking at total hemozoin content, there is more hemozoin in the liver until day 10 post treatment as compared to the spleen. Where we see a switch in liver and spleen concentrations when normalized to tissue size, we do not see this reflected in total hemozoin content. It appears that around day 13, the total amount of hemozoin present in the spleen is the same as that of the liver. Studies have shown hemozoin to persist in tissue as far as 9 months post clearance which we were also able to demonstrate with quantifiable amounts of hemozoin in the liver and spleen at day 100 post clearance.

In whole blood, we expect to see the greatest amount of hemozoin at day 0 because the mice have reached a peak parasitemia of infection. The curative dose of pyronaridine at day 0 is reflected in the rapid decline of hemozoin concentration between days 0-4 as parasite numbers are drastically reduced due to drug treatment. Around the same time we see a switch between liver and spleen concentrations, we see a rapid increase of hemozoin in whole blood. This may represent clearance of parasites from the liver to the spleen via the whole blood. Parasite clearance from blood occurs at day 6 by qPCR. Therefore, an increase in spleen concentration around this time may correspond to clearance of parasites in the blood through the spleen. The peak at day 10 in whole blood also corresponds to the decrease in total hemozoin content in the liver and lower levels in

the spleen. Therefore, we assume that most of the hemozoin is in the blood at this time point. As clearance continues through to day 13, hemozoin levels decline in the whole blood, liver and spleen. Hemozoin concentrations in the spleen after day 13 are represented with an N of at least 10 mice, therefore, we are confident in these values. However, we only processed livers from 3-5 mice for each group and would need to process more to confirm our current values for hemozoin concentration in the liver. We would also like to see whether the unexpected increase at day 86 is an artifact or caused by a recurrence of parasitemia.

In the study by Pisciotta et. al., hemozoin was not detected in up to 320 ul of plasma from mouse whole blood [7]. However, with our sensitive luminol assay, we were able to quantify hemozoin in both RBC and plasma fractions of whole blood from *Plasmodium* infected mice and human patients. In mice, we see rapid clearance of hemozoin from the RBC fraction, synchronous to whole blood. Although the trends are similar between WB and RBC hemozoin concentrations at days 0-2, a higher RBC concentration may reflect that we purified hemozoin from packed RBCs resulting in a higher hematocrit comparatively to WB. At days 0-2, there is significantly higher amounts of hemozoin in the RBC fraction as compared to plasma. This may represent the large numbers of trophozoite-infected RBCs being cleared from the whole blood immediately after drug treatment. Between days 7-13, however, we do not see a significant difference in the RBC and plasma levels of hemozoin. However, a higher percentage of plasma samples were able to be positively quantified at days 7-13 than RBC samples. This may indicate a shift towards hemozoin remaining in the plasma considering the unwashed RBC pellet may also account for hemozoin-containing WBCs.

Long term hemozoin concentrations in these fractions cannot be determined by our analysis because we only had 1 positive sample in both fractions at day 100. Therefore, we would need to perform more long term mouse experiments to determine if there is residual hemozoin in the plasma after RBC clearance post day 13. Calculation of the ratio of hemozoin in RBC to plasma fractions resulted in a range of 2-fold to 20,000-fold and does not remain consistent over the course of clearance nor within a group of mice on a single day.

The implication of this research is to understand hemozoin kinetics in humans. Therefore, we looked at hemozoin concentrations within the washed RBC and plasma fractions of patients infected with *Plasmodium*. Although limited in the number of samples and duration post treatment, we saw more hemozoin in the RBC fraction in all but one of the samples. This reflects what was observed in the mice, where more hemozoin was present in the RBC fraction of mouse samples. Because we only had 1-3 patient samples per time point, it is difficult to say whether the trends seen during clearance of infection in humans are of any biological significance. However, we did observe a rapid decline of hemozoin concentration up to 2 days post treatment as parasites are being cleared from the blood, similar to what occurred in the mice.

We were able to quantify hemozoin in fewer patient samples as compared to mice relative to the total number of samples processed. This may be due to the limitations of human blood collection. Mouse blood was taken via cardiac puncture, and therefore yielded dispensable volumes for us to work with. The human samples were from peripheral blood which generally have lower amounts of trophozoites due to their nature of sequestration. Therefore, it is possible that we were quantifying hemozoin production

from ring stage parasites but were not accurately capturing total hemozoin concentration due to the limited number of circulating trophozoites in peripheral blood. This can be confirmed by comparing hemozoin concentrations to the specific life cycle stages of *Plasmodium* in our patient samples. Because our patient RBC pellets were washed, we theoretically removed any hemozoin containing WBCs, giving us a more accurate measure of RBC hemozoin content. We would like to continue to process more patient samples, preferably at consistent time points during the first two weeks of clearance to replicate the kinetics we see in mice. With a sensitive luminescence assay, we can continue to quantify hemozoin in *Plasmodium* infect patients to truly determine the kinetics of hemozoin within the RBC and plasma compartments of human whole blood.

REFERENCES

1. Grimberg BT, Grimberg KO. Hemozoin detection may provide an inexpensive, sensitive, 1-minute malaria test that could revolutionize malaria screening. Expert Rev Anti Infect Ther. 2016;14:879–83.

2. Sullivan DJ. Theories on malarial pigment formation and quinoline action. Int J Parasitol. 2002;32:1645–53.

3. Olivier M, Van Den Ham K, Shio MT, Kassa FA, Fougeray S. Malarial pigment hemozoin and the innate inflammatory response. Front Immunol. 2014;5:1–10.

4. Sullivan A, I I, Meshnick S. Patterns of hemozoin accumulation in tissue.pdf. Parasitology. 1995;112:285–94.

5. Levesque M, Sullivan A, Meshnick S. Splenic and hepatic hemozoin in mice after malaria parasite clearance. J Parasitol. 1999;85:570–3.

6. Frita R, Carapau D, Mota MM, Hänscheid T. *In vivo* hemozoin kinetics after clearance of *Plasmodium berghei* infection in mice. Malar Res Treat. 2012;2012:1–9.

7. Pisciotta JM, Scholl PF, Shuman JL, Shualev V, Sullivan DJ. Quantitative characterization of hemozoin in *Plasmodium berghei* and *vivax*. Int J Parasitol Drugs Drug Resist [Internet]. Elsevier Ltd; 2017;7:110–9. Available from: http://dx.doi.org/10.1016/j.ijpddr.2017.02.001

8. Deroost K, Lays N, Noppen S, Martens E, Opdenakker G, Van Den Steen PE. Improved methods for haemozoin quantification in tissues yield organ-and parasite-specific information in malaria-infected mice. Malar J [Internet]. Malaria Journal; 2012;11:1. Available from: Malaria Journal

Abeer A. Sayeed

Curriculum Vitae

abeerafnan@gmail.com | (508) 736-1445

EDUCATION

Expected May 2019

Master of Science (ScM)
Molecular Microbiology & Immunology
Johns Hopkins Bloomberg School of Public Health, Baltimore, MD
Thesis: *Analyzing the morphology of hemozoin in drug resistant Plasmodium & quantifying the compartmental kinetics of hemozoin during clearance of infection*

Aug. 2014

Bachelor of Science (B.S.)
Biology
Northeastern University, Boston, MA
Senior Capstone: *Exploring the hydrophobic pocket on apical membrane antigen 1 (AMA1) within Plasmodium species*

RESEARCH EXPERIENCE

Jan. 2018 – Present

Graduate Student
Sullivan Lab, Dept. of Molecular Microbiology & Immunology
Johns Hopkins Bloomberg School of Public Health, Baltimore, MD

- Develop and optimize a novel, sensitive luminescence assay to quantify hemozoin in fractionated blood from *Plasmodium* infected samples
- Analyze kinetics of hemozoin during blood stage infection by comparing hemozoin quantities between RBC and plasma fractions
- Culture and drug treat parasites to isolate, purify, and image (FEISEM) hemozoin
- Explore hemozoin production as a parasite stress response by measuring and comparing hemozoin dimensions between isogenic and non-isogenic, sensitive and resistant *Plasmodium* strains

Jan. 2015 – Jun. 2017

Research Associate II
Cancer Cell Line Factory, Boehm Lab, Cancer Program
Broad Institute of MIT and Harvard, Cambridge, MA

- Generated novel patient-derived cancer cell models, responsible for melanoma and pediatric cancer cohorts
- Developed and refined a robust pipeline for cell culture initiation, genomic verification, and culture scale-up
- Lead efforts to establish automation pipeline for processing high-throughput DNA extraction, quantification, and normalization
- Cultured rare cancer samples using novel systematic approach, in up to 64 media conditions per sample to increase cell line take rate
- Tracked and recorded initiation attempts, success rates, and take rates for over 200 pediatric cancer samples to build a pediatric cancer cell culture database for real-time reference
- Performed DNA/RNA extractions from blood/cells/tissue, cell line fingerprinting, mycoplasma testing, and cell viability assessments
- Prepared, ordered, and maintained necessary reagents, solutions, and lab supplies for efficient operation of team space
- Collaborated with team and cohort champions to plan experiments and shared results in team meetings and conferences

Jan. 2014 – Jun. 2014 **Co-op Research Assistant**
Discovery Biology
Shire Human Genetic Therapies, Inc.

- Cultured and maintained human epithelial mesothelioma cell line (H2452)
- Performed RNA extractions from muscle tissue, RT-PCR, ELISA & MSD assays on mouse urine and serum samples, cell proliferation assays, cell staining, and imaging
- Collected total protein, creatinine, and blood urea nitrogen concentrations in mouse urine and serum samples on the cobas c 311 chemistry analyzer
- Participated in mouse tissue collection for studies, including blood perfusions and cardiac punctures
- Practiced IP/IV injections and urine collection on live mice, and IT injections on euthanized mice
- Participated in discovery research discussions for rare genetic diseases and presented results during team meetings

Jul. 2013 – Aug. 2013 **Intern Research Assistant**
Jacobson Lab, Dept. of Microbiology & Physiological Systems
University of Massachusetts Medical School, Worcester, MA

- Isolated, amplified, and transformed *Upf* gene deletions tagged with Sup45-SNAP in yeast
- Measured *Renilla* and Firefly luciferase in yeast using dual luciferase assays
- Calculated and presented doubling times and nonsense codon readthrough to determine effects of Sup45-SNAP on premature translation termination

Jan. 2011 – Dec. 2013 **Undergraduate Research Assistant**
Humic Acid Research Group, Dept. of Chemistry
Northeastern University, Boston, MA

- Collected spectrophotometric data to measure fulvic acid levels in National Soil Project samples

LEADERSHIP EXPERIENCE

Nov. 2018 – Present **Teaching Assistant**
Johns Hopkins Bloomberg School of Public Health, Baltimore, MD
Course Titles: Public Health Perspectives in Research, Public Health Biology

- Facilitate live interactive session and grade writing assignments

Sep. 2017 – Present **Student Group Social Coordinator**
Dept. of Molecular Microbiology & Immunology
Johns Hopkins Bloomberg School of Public Health, Baltimore, MD

- Organize monthly departmental social events and annual welcome events for new students

Sep. 2018 – Present **Student-Faculty Liaison**
Dept. of Molecular Microbiology & Immunology
Johns Hopkins Bloomberg School of Public Health, Baltimore, MD

- Attend monthly faculty meetings to communicate student group needs and updates

Jun. 2016 – Aug. 2016 **Broad Summer Scholars Program Mentor**

Broad Institute of MIT & Harvard, Boston, MA

- Mentored and trained a high school summer student on live-cell imaging and growth rate calculation of a pediatric BRD4-NUT midline carcinoma to optimize in vitro growth conditions and maintain tumor genetic profile

PUBLICATIONS

Andrew Hong, Yuen-Yi Tseng, Gabriel Sandoval, Jeremiah Wala, Won Jun Kim, Bryan Kynnap, Mihir Doshi, Guillaume Kugener, Thomas Howard, Ji Li, Xiaoping Yang, Michelle Tillgren, Mahmoud Ghandi, **Abeer Sayeed**, Rebecca Deasy, Abigail Ward, Brian McSteen, Katherine Labella, Paula Keskula, Adam Tracy, Cora Connor, Catherine Clinton, Alanna Church, Brian Crompton, Katherine Janeway, Barbara Van Hare, David Sandak, Ole Gjoerup, Pratiti Bandopadhayay, Paul Clemons, Stuart Schreiber, David Root, Prafulla Gokhale, Susan Chi, Elizabeth Mullen, Charles Roberts, Cigall Kadoch, Rameen Beroukhim, Keith Ligon, Jesse Boehm, and William Hahn. (2019) Renal medullary carcinomas depend upon SMARCB1 loss and are sensitive to proteasome inhibition. *eLife.* e44161. doi: 10.7554/eLife.44161

Elham A. Ghabbour, Geoffrey Davies, **Abeer A. Sayeed**, Millicent T. Croman, Brittney A. Hoehing, Edward Ayres (2015). Measuring the total and sequestered organic matter contents of grassland and forest soil profiles in the National Ecological Observatory Network initiative. *Soil Horizons*. 56: 1-11. doi:10.2136/sh15-07-0014

Elham A. Ghabbour, Geoffrey Davies, **Abeer A. Sayeed**, Tony Jenkins (2013). Measuring the retained water and sequestered organic carbon contents of soil profiles in Aroostook and Piscataquis counties, Maine, USA. *Soil Horizons* 54: 1-7. doi:10.2136/sh13-05-0012

ABSTRACTS

Abeer Sayeed, David Sullivan. Hemozoin in isogenic drug resistant *P. falciparum* is smaller in size. Presented at the Annual Future of Malaria Symposium, Rockville, MD, 2018.

Abeer Sayeed, David Sullivan. Hemozoin in isogenic drug resistant *P. falciparum* is smaller in size. Presented at the Annual Molecular Parasitology Meeting, Woods Hole, MA, 2018.

Yuen-Yi (Moony) Tseng, Andrew Hong, Shubhroz Gill, Paula Keskula, Srivatsan Raghavan, Jaime Cheah, Aviad Tsherniak, Francisca Vazquez, Sahar Alkhairy, Anson Peng, **Abeer Sayeed**, Rebecca Deasy, Peter Ronning, Philip Kantoff, Levi Garraway, Mark Rubin, Calvin Kuo, Sidharth Puram, Adi Gazdar, Nikhil Wagle, Adam Bass, Keith Ligon, Katherine Janeway, David Root, Stuart Schreiber, Paul Clemons, Todd Golub, William Hahn and Jesse Boehm. Expanding tumor chemical-genetic interaction map using next generation cancer models. Presented at American Association for Cancer Research Precision Medicine Series, San Jose, CA, 2017.

Andrew L. Hong, Yuen-Yi Tseng, Bryan D. Kynnap, Mihir B. Doshi, Gabriel Sandoval, Coyin Oh, **Abeer Sayeed**, Gill Shubhroz, Alanna J. Church, Paula Keskula, Anson Peng, Paul A. Clemons, Aviad Tsherniak, Francisca Vazquez, Carlos Rodriguez-Galindo, Katherine A. Janeway, Levi A. Garraway, Stuart L. Schreiber, David E. Root, Elizabeth Mullen, Kimberly Stegmaier, Cigall Kadoch, Charles W.M. Roberts, Jesse S. Boehm

and William C. Hahn. Identification of druggable targets through functional multi-omics in renal medullary carcinoma. Presented at American Association for Cancer Research Precision Medicine Series, San Jose, CA, 2017.

Yuen-Yi Tseng, Andrew Hong, Paula Keskula, Shubhroz Gill, Jaime Cheah, Grigoriy Kryukov, Aviad Tsherniak, Francisca Vazquez, Glenn Cowley, Sahar Alkhairy, Coyin Oh, Anson Peng, Rebecca Deasy, **Abeer Sayeed**, Peter Ronning, Samuel Ng, Steven Corsello, Corrie Painter, David Sandak, Levi Garraway, Mark Rubin, Calvin Kuo, Sidharth Puram, David Weinstock, Adam Bass, Nikhil Wagle, Keith Ligon, Katherine Janeway, David Root, Stuart Schreiber, Paul Clemons, Aly Shamji, Aly Shamji, William Hahn, Todd Golub and Jesse Boehm. Accelerating prediction of pediatric and rare cancer vulnerabilities using next-generation cancer models. Presented at the Annual American Association for Cancer Research Meeting, Washington DC, 2017.

Yuen-Yi Tseng, Andrew Hong, Paula Keskula, Shubhroz Gill, Jaime Cheah, Grigoriy Kryukov, Aviad Tsherniak, Francisca Vazquez, Glenn Cowley, Coyin Oh, Anson Peng, **Abeer Sayeed**, Rebecca Deasy, Peter Ronning, Philip Kantoff, Levi Garraway, Mark Rubin, Calvin Kuo, Sidharth Puram, Adi Gazdar, Filemon Dela Cruz, Adam Bass, Nikhil Wagle, Keith Ligon, Katherine Janeway, David Root, Stuart Schreiber, Paul Clemons, Aly Shamji, William Hahn, Todd Golub and Jesse S. Boehm. Accelerating prediction of tumor vulnerabilities using next-generation cancer models. Presented at the Annual American Association for Cancer Research Meeting, New Orleans, LA, 2016.

Elham A. Ghabbour, Geoffrey Davies, **Abeer A. Sayeed**, Millicent T. Croman and Edward Ayres. Measuring Sequestered Carbon Contents of Grassland and Forest Soil Profiles in the NEON Initiative. Presented at the Annual International Conference of the Soil Science Society of America, Long Beach, CA, 2014.

Elham Ghabbour, Geoffrey Davies, **Abeer Sayeed** and Tony Jenkins. Measuring the Retained Water and Sequestered Organic Carbon Contents of Soil Profiles in Aroostook and Piscatiquis Cos, Maine, USA. Presented at the Biennial National Soil Survey Conference, Annapolis, MD, 2013.

Elham Ghabbour, Geoffrey Davies, **Abeer Sayeed** and Tony Jenkins. Measuring the Retained Water and Sequestered Organic Carbon Contents of Soil Profiles in Aroostook and Piscatiquis Cos, Maine, USA. Presented at the Research, Innovation, and Scholarship Expo at Northeastern University, Boston, MA, 2013.